SECTION 2.3
CENTRIFUGAL PUMP PERFORMANCE

2.3.1 CENTRIFUGAL PUMPS: GENERAL PERFORMANCE CHARACTERISTICS

C. P. KITTREDGE
PAUL COOPER

DEFINITIONS

Nomenclature Many of the quantities involved in this subsection are also dealt with in Section 2.1. Therefore, a single nomenclature that applies to both sections appears at the beginning of Section 2.1. Differences in notation exist for some of these quantities as a result of the coexistence of different traditions and pump cultures, so the nomenclature shows the equivalence in each case. An example is the use in this subsection of "c" and "w" to denote absolute and relative velocity respectively, whereas the NASA system of capital letters V and W is employed in Section 2.1.

Units The units used in this subsection are as defined in the nomenclature unless specifically noted in the text. In particular, the primary units for this subsection are those of the U.S. Customary System (USCS). A distinction in USCS usage in this subsection is that the pound force (lbf) is represented simply as "lb". In keeping with the commentary on SI units in the front matter of this handbook, conversions to SI units are given throughout this subsection, or the actual equivalent SI values are given in parentheses.

However, the number appearing in parentheses after the USGS value of specific speed n_s is the equivalent value of the universal specific speed Ω_s. Note that the value of specific speed corresponding to the best efficiency point (BEP) operating conditions of the pump is the value of interest and is often used to identify the impeller geometry involved.

Volume Flow Rate Abbreviated to "flow rate" and known traditionally as "pump capacity" Q, this is the volume of liquid per unit time delivered by the pump. In USCS units, Q is expressed in U.S. gallons per minute or USgpm, for which the abbreviation "gpm" is

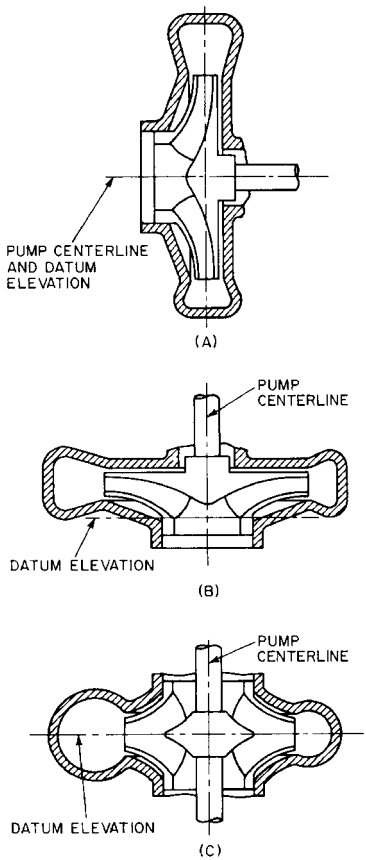

FIGURE 1A through C Elevation datum for defining pump head (Hydraulic Institute ANSI/HI 2000 Edition Pump Standards, Reference 27)

used. (1 US gallon = 231 in^3.) For very large pumps, the units ft^3/sec are used. The consistent SI units m^3/s are implied when an SI value of Q is—unless the numerically convenient liters per second (l/s) are specifically called out.

Datum for Pump Head As defined in Eq. 3 and Figure 1 of Section 2.1, the total head has components of pressure, velocity, and elevation Z (or Z_e). Because pump head H (more precisely ΔH) is the difference of the total heads evaluated at the discharge flange d and the suction flange s respectively, the elevation of the datum from which Z is measured cancels out. However, for purposes of identification, computing NPSH, and so on, the standard datum as shown in Figure 1 is used.

The standard datum for horizontal-shaft pumps is a horizontal plane through the centerline of the shaft (Figure la). For vertical-shaft pumps, the datum is a horizontal plane through the entrance eye of the first-stage impeller (Figure lb) if single suction or through the centerline of the first stage impeller (Figure 1c) if double suction. Because pump head is the difference between the discharge and suction heads, it is not necessary that the standard datum be used, and any convenient datum may be selected for computing the pump head.

Power In USCS, the pump output is customarily given as liquid horsepower (lhp) or as water horsepower if water is the liquid pumped. It is given by

$$lhp = \frac{QH(\text{sp. gr.})}{3960} \tag{1}$$

where Q is in gallons per minute, H is in feet, and sp. gr. is specific gravity. If Q is in cubic feet per second, the equation becomes

$$lhp = \frac{QH(\text{sp. gr.})}{8.82} \tag{2}$$

In SI, the power P in watts (W) is given by

$$P = 9797QH\ (\text{sp. gr.}) \tag{3}$$

where Q is in cubic meters per second and H is in meters.

When Q is in liters per second and H is in meters

$$P = 9.797QH\ (\text{sp. gr.}) \tag{4}$$

Efficiency The pump efficiency η is the liquid horsepower divided by the power input to the pump shaft. The latter usually is called the brake horsepower (bhp). The efficiency may be expressed as a decimal or multiplied by 100 and expressed as percent. In this subsection, the efficiency will always be the decimal value unless otherwise noted. Some pump driver-units are so constructed that the actual power input to the pump is difficult or impossible to obtain. Typical of these is the "canned" pump for volatile or dangerous liquids. In such case, only an *overall efficiency* can be obtained. If the driver is an electric motor, this is called the *wire-to-liquid efficiency* or, when water is the liquid pumped, the *wire-to-water efficiency.*

CHARACTERISTIC CURVES

Pump with Non-Viscous Flow and Zero Slip The basic shapes of centrifugal pump performance characteristics arising from various geometries can be ascertained and compared without the necessity of evaluating the slip. (Illustrated in Figure 15 of Section 2.1, the slip phenomenon is explained in the related discussion[1].) For this purpose, one employs the artifice of non-viscous flow through an impeller with an infinite number of blades having infinitesimal thickness and that therefore produce neither structural (geometric) nor flow (boundary layer) blockage. The result is the ideal head for no slip or blockage H_e as given by Eq. 5 (cf. Eq. 15b of Section 2.1):

$$H_e = \frac{u_2 c_{u2}}{g} - \frac{u_1 c_{u1}}{g} \tag{5}$$

The velocity components in Eq. 5 can be seen in the velocity diagrams of Figure 2, slip being neglected. Generally the inlet swirl term is small, and Eq. 5 can be approximated by

$$H_e \cong \frac{u_2 c_{u2}}{g} \tag{6}$$

As shown in Figure 2b, the absolute velocity vector c may be resolved into the meridional, or radial, velocity c_m and the peripheral velocity c_u. From the geometry of the figure

$$c_{u2} = u_2 - \frac{c_{m2}}{\tan \beta_2} \tag{7}$$

which, substituted into Eq. 6, gives

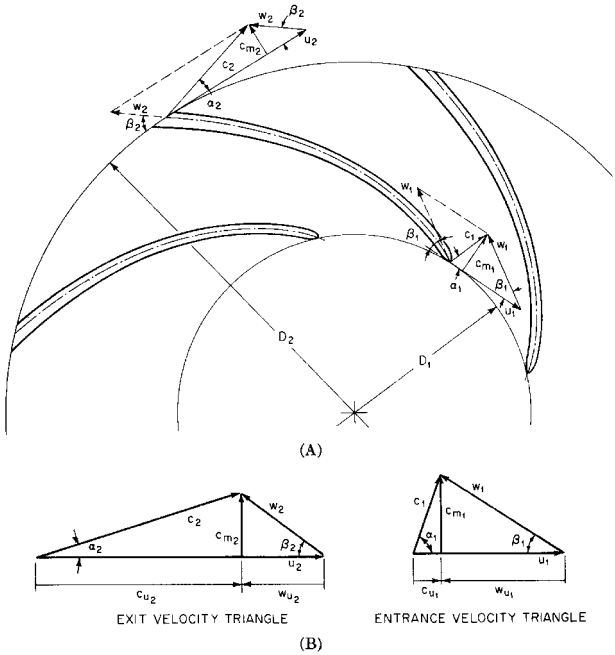

FIGURE 2A and B Velocity diagrams for radial-flow impellers, neglecting slip and blockage

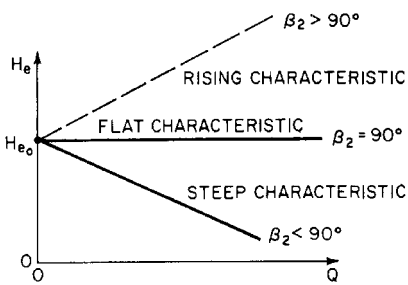

FIGURE 3 Head-versus-flow rate characteristics for non-viscous, zero-slip impeller flow

$$H_e = \frac{u_2^2}{g} - \frac{u_2 c_{m2}}{g \tan \beta_2} \tag{7}$$

Neglecting leakage flow, the meridional velocity c_m must be proportional to the capacity Q. With the additional assumption of constant impeller speed, Eq. 8 becomes

$$H_e = k_1 - k_2 Q \tag{8}$$

in which k_1 and k_2 are constants, with the value of k_2 dependent on the value of the vane angle β_2. Figure 3 shows the $H_e - vs - Q$ characteristics for the three possible conditions on the vane angle at exit β_2. The second right-hand term in Eq. 5 may be treated in like manner to the foregoing and included in Eqs. 8 and 9. The effect on Figure 3 would be to change

the value of $H_e = u_2^2/g$ at $Q = 0$ and the slopes of the lines, but all head-flow rate characteristics would remain straight lines.

Viscous Flow with Slip The real flow situation involves friction losses in an impeller with a finite number of relatively widely spaced blades. Thus, slip occurs, reducing the exit flow angle β_{f2} below that of the blade β_2, (or, more precisely, $\beta_{b,2}$,) which in turn reduces c_{u2} (cf. Figure 15 of Section 2.1). Therefore, the ideal head H_i drops below H_e. Moreover, losses and recirculation occur to cause additional deviation of pump head H from H_e. While CFD flow analysis can be employed to predict H with fair accuracy[2], lesser means, such as one-dimensional analysis, require experienced correlation and calibration skills to make such predictions. Therefore, many engineers commonly depend on testing and empirical modification of test results on the exact or similar geometry to make the final determination of the performance characteristics of a pump. This effort involves constant-speed plots of data as shown in the example of Figure 4.

Pumps are designed to operate at the point of best efficiency. The head, power, and flow rate at best efficiency, often called the *normal* values, are indicated in this subsection by H_n, P_n, and Q_n respectively. Sometimes a pump may be operated continuously at a flow rate slightly above or below Q_n. In such case, the actual operating point is called the *rated* or *guarantee* point if the manufacturer specified this capacity in the guarantee. It is unusual to operate a pump continuously at a flow rate at which the efficiency is much below the maximum value. Apart from the unfavorable economics, the pump may be severely damaged by continued off-design operation, as described later.

Backward-Curved Blades, $\beta_2 < 90°$ Figure 4 shows the characteristics of a double-suction pump with backward-curved blades, $\beta_2 = 23°$. The impeller discharged into a single volute casing, and the specific speed was $n_s \approx 2200$ ($\Omega_s \approx 0.8$) at best efficiency. At shutoff ($Q = 0$), Eq. 8 predicts H_e to be 374 ft (114 m), whereas the pump actually developed about 210 ft (64 m), and this head remained nearly constant for the range $0 < Q < 1000$ gpm (63 l/s). For $Q > 1000$ gpm (63 l/s), the head decreased with increasing capacity but not in the linear fashion predicted by Eq. 9. At best efficiency, where $Q_n = 3200$ gpm (202 l/s), Eq. 8 predicts $H_e = 281$ ft (86 m), whereas the pump actually developed $H_n = 164$ ft (50 m).

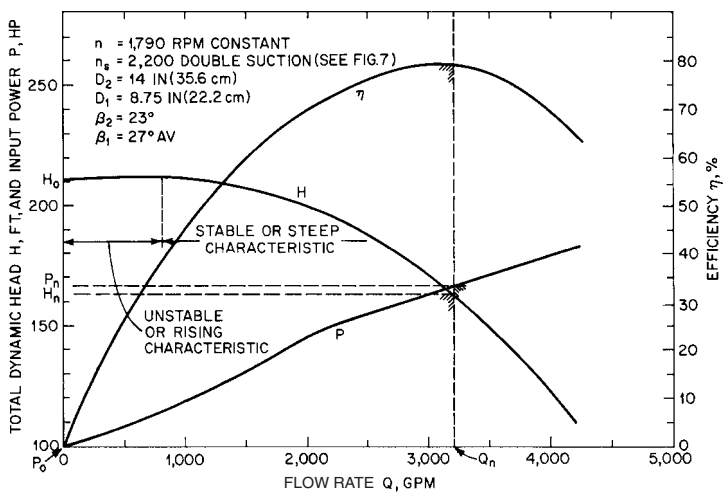

FIGURE 4 Typical pump characteristics, backward-curved blades (ft × 0.3048 = m; hp × 745.7 = W; gpm × 0.06309 = l/s)

Radial Blades, $\beta_2 = 90°$ Large numbers of radial-blade pumps are used in many applications, from cellar drainers, cooling-water pumps for internal combustion engines, and other applications where low first cost is more important than high efficiency to highly engineered pumps designed for very high heads. The impellers are rarely more than 6 in (15 cm) in diameter, but the speed range may be from a few hundred to 30,000 rpm or more. The casings usually are concentric with the impellers and have one or more discharge nozzles that act as diffusers. The impellers usually are open, with three or more flat blades. The clearance between blades and casing is relatively large for easy assembly. Such pumps exhibit a flat head-capacity curve from shutoff to approximately 75% of best efficiency flow rate, and beyond this flow the head-flow curve is steep. The pumps develop a higher head, up to 8000 ft (2400 m) per stage, than pumps with backward-curved blades, but the efficiency of the former usually is lower. (See also Subsection 2.2.1.)

Figure 5 shows the characteristics of a pump as reported by Rupp.[3] The impeller was fully shrouded, $D = 5.25$ in (13.3 cm), and fitted with 30 blades of varying length. The best efficiency, $\eta = 55\%$, was unusually high for the specific speed $n_s = 475$ (0.174), as may be seen from Figure 6. The head-flow curve showed a rising (unstable) characteristic for $0 < Q < 25$ gpm (1.6 l/s) and a steep characteristic for $Q > 25$ gpm (1.6 l/s).

Figure 7 shows the characteristics of a pump as reported by Barske.[4] The impeller was open, $D \approx 3$ in (7.6 cm), and fitted with six radial tapered blades. The effective β_2 may have been slightly greater than 90° due to the taper. At 30,000 rpm, the best efficiency was more than 35% at $n_s = 355$ (0.130), which is much higher than for a conventional pump of this specific speed and capacity (Figure 6). The head-flow curve showed a nearly flat characteristic over most of the usable range, as predicted by Eq. 8, but the head was always lower than H_e. The smooth concentric casing was fitted with a single diffusing discharge nozzle. When two or more nozzles were used, the head-flow curves showed irregularities at low flow rates and became steep at high flow rates.

Manson[5] has reported performance characteristics for jet engine fuel pumps having straight radial blades in enclosed impellers. The head curves showed unstable characteristics at low flow rates and steep characteristics at higher flow rates. The best efficiency reported was 54.7% for an impeller diameter of 3.300 in (8.382 cm) and speed $n =$ 28,650 rpm.

Forward-Curved Blades, $\beta_2 > 90°$ Pumps with forward-curved blades have been proposed,[6] but the research necessary to achieve an efficient design appears never to have been carried out. Tests have been made of conventional, backward-curved-blade, double-suction pumps with the impellers mounted in the reversed position but with rotation correct for the volute casing. As tested, these pumps therefore had forward-curved blades.

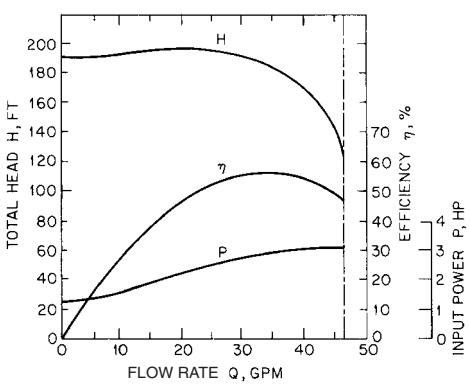

FIGURE 5 Pump characteristics, radial blades (ft × 0.3048 = m; hp × 745.7 = W; gpm × 0.06309 = l/s) (Reference 3)

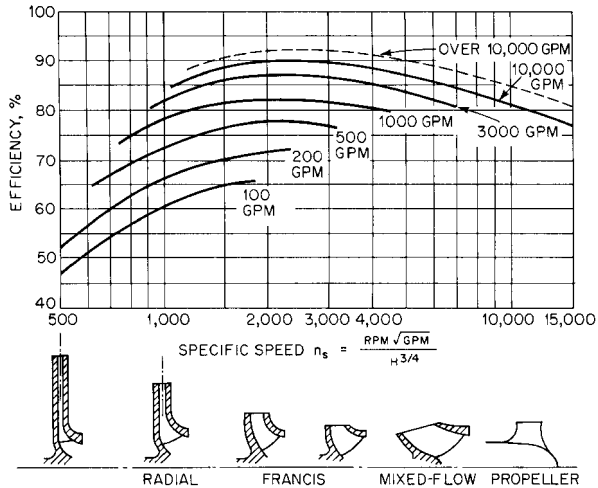

FIGURE 6 Pump efficiency versus specific speed and size (gpm × 0.06309 = l/s) (Flowserve Corporation) ($\Omega_s = n_s/2733$)

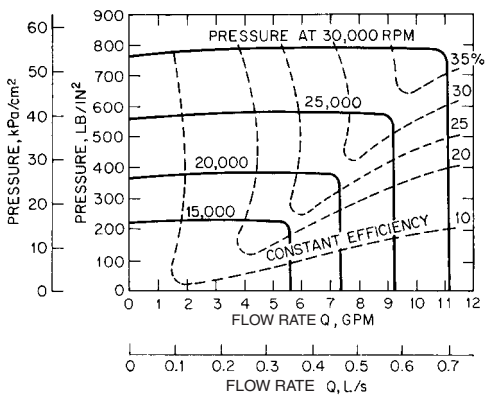

FIGURE 7 Pump characteristics, radial blades (lb/in² × 6.894 = kPa; gpm × 0.06309 = l/s) (Reference 4)

Table 1 shows the pertinent results for six different pumps. Both flow rate and efficiency were drastically reduced, and there was only a modest increase in head for five of the six pumps. The sixth pump showed a 38% increase in head over that obtained with the impeller correctly mounted. Published estimates[7,8] of the head-flow curves to be expected from reversed impellers predict an unstable characteristic at the low end of the flow rate range and a steep characteristic at the high end of the range.

PERFORMANCE EFFECTS

Classification of Curve Shapes A useful method for comparing characteristics of pumps of different specific speeds is to normalize on a selected operating condition, usually best efficiency. Thus,

TABLE 1 Effects of reversed mounting of impeller

Number of stages	Specific speed per stage n_s (Ω_s)	Percent of normal shutoff head	Percent of normal values at best efficiency			
			Head	Flow Rate	Power	Efficiency
2	828 (0.303)	86	111	65	104	71
2	1024 (0.375)	82	112	88	145	68
1	1240 (0.454)	75	105	38.5	68.5	59
1	1430 (0.523)	82	106	69.7	138	53.5
1	2570 (0.940)	74.5	117	62	138	52.5
1	2740 (1.003)	77.5	138	61.5	180	47

Source: Flowserve Corporation

$$q = \frac{Q}{Q_n} \quad h = \frac{H}{H_n} \quad p = \frac{P}{P_n} \tag{10}$$

where the subscript n designates values for the best efficiency point. Figures 8, 9, and 10 show approximate performance curves normalized on the conditions of best efficiency and for a wide range of specific speeds as defined in Table 2. These curves are applicable to pumps of any size because absolute magnitudes have been eliminated. In Figure 8, curves 1 and 2 exhibit a *rising head* or *unstable* characteristic where the head increases with increasing flow rate over the lower part of the flow rate range. This may cause instability at heads greater than the shutoff value, particularly if two or more pumps are operated in parallel. Curve 3 exhibits an almost constant head at low flow rates and is often called a *flat* characteristic. Curves 4 to 7 are typical of a *steep* or *stable head* characteristic, in which the head always decreases with increasing flow rate. Although the shape of the head-flow curve is primarily a function of the specific speed, the designer has some control through selection of the vane angle β_2 number of impeller vanes n_b, and capacity coefficient $\phi = c_{m2}/u_2$, as described in Section 2.1 (see also Figure 2). For pumps having a single-suction specific speed approximately 5000 (1.83) and higher, the power is at its maximum at shutoff and decreases with increasing flow rate. This may require an increase in the power rating of the driving motor over that required for operation at normal capacity.

Efficiency The efficiency η is the product of three component efficiencies (defined in Section 2.1):

$$\eta = \eta_m \eta_v \eta_h \tag{11}$$

The mechanical efficiency η_m accounts for the bearing, stuffing box, and all disk-friction losses including those in the wearing rings and balancing disks or drums if present. The volumetric efficiency η_v accounts for leakage through the wearing rings, internal labyrinths, balancing devices, and glands. The hydraulic efficiency η_h accounts for liquid friction losses in all through-flow passages, including the suction elbow or nozzle, impeller, diffusion vanes, volute casing, and the crossover passages of multistage pumps. Figure 11 shows an estimate of the losses from various sources in double-suction single-stage pumps having at least 12-in (30-cm) discharge pipe diameter. Minimum losses and hence maximum efficiencies are seen to be in the vicinity of $n_s \approx 2500$ (0.91), which agrees with Figure 6.

Effects of Pump Speed Increasing the impeller speed increases the efficiency of centrifugal pumps. Figure 7 shows a gain of about 15% for an increase in speed from 15,000 to 30,000 rpm. The increases are less dramatic at lower speeds. For example, Ippen[9] reported about 1% increase in the efficiency of a small pump, $D = 8$ in (20.3 cm) and $\eta_s = 1992$ (0.73), at best efficiency, for an increase in speed from 1240 to 1880 rpm. Within limits, the cost of the pump and driver usually decreases with increasing speed. Abrasion

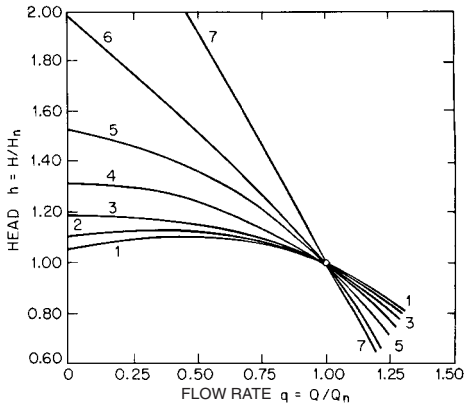

FIGURE 8 Head curves for several specific speeds, as defined in Table 2 (Reference 12)

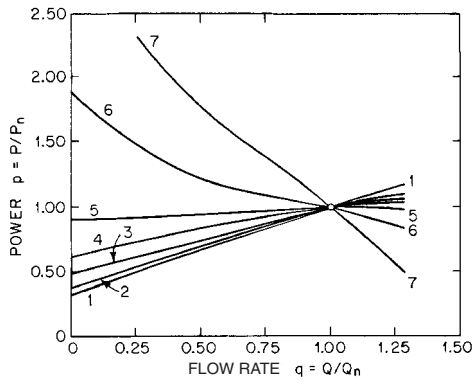

FIGURE 9 Power curves for several specific speeds, as defined in Table 2 (Reference 12)

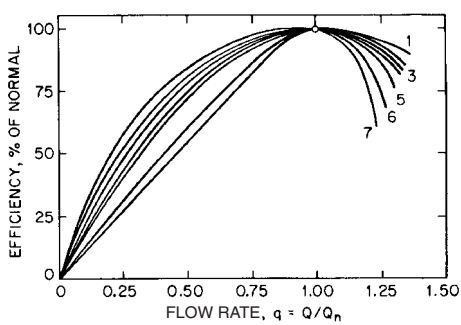

FIGURE 10 Efficiency curves for several specific speeds, as defined in Table 2 (Reference 12).

TABLE 2 Characteristic curves as a function of specific speed (Figures 8, 9, and 10)

Curve Number on Figures 8 , 9 , and 10	USCS Specific Speed n_s	Metric (SI) Specific Speed n_q	Universal Specific Speed Ω_s	Impeller Suction Configuration
1	900	17	0.33	Double
2	1500	29	0.55	Double
3	2200	43	0.80	Double
4	3000	58	1.10	Double
5	4000	77	1.46	Double
6	5700	110	2.09	Single
7	9200	178	3.37	Single

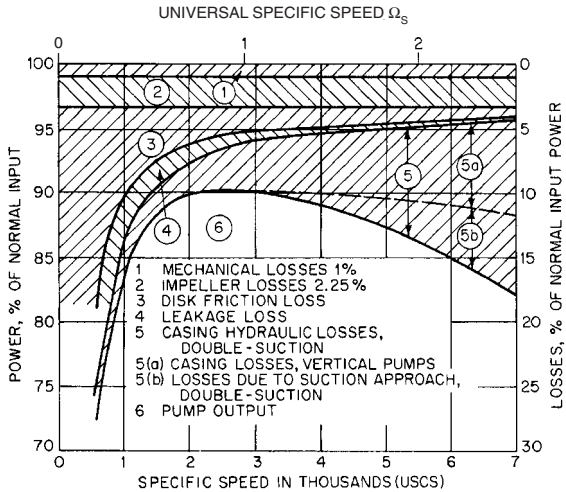

FIGURE 11 Power balance for double-suction pumps at best efficiency (Reference 12)

and wear increase with increasing speed, particularly if the liquid contains solid particles in suspension. The danger of cavitation damage usually increases with increasing speed unless certain suction requirements can be met, as described later.

Effects of Specific Speed Figues 6 and 11 show that maximum efficiency is obtained in the range 2000 (0.73) $< n_s <$ 3000 (1.10), but this is not the only criterion. Pumps for high heads and small flow rates occupy the range 500 (0.18) $< n_s <$ 1000 (0.37). At the other extreme, pumps for very low heads and large flow rates may have n_s = 15,000 (5.49) or higher. For given head and flow rate, the pump having the highest specific speed that will meet the requirements probably will be the smallest and least expensive. However, Figure 9 of Section 2.1 shows that it will run at the highest speed and be subject to maximum wear and cavitation damage, as previously mentioned.

Effects of Clearance

WEARING-RING CLEARANCE Details of wearing-ring construction are given in Subsection 2.2.1. Schematic outlines of two designs of rings are shown in Figure 12. The L-shaped construction shown in Figure 12a is very widely used with the close clearance between the cylindrical portions of the rings. Leakage losses increase and pump performance

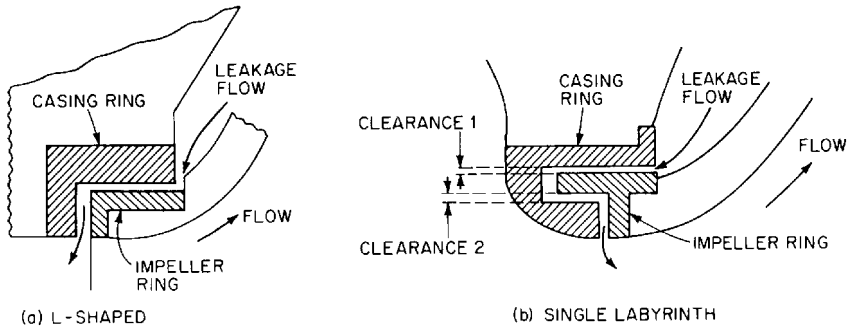

FIGURE 12A and B Typical wearing rings

TABLE 3 Effects of increased wearing-ring clearance on centrifugal pump performance

Specific speed n_s (Ω_s)	Design head, ft (m)	Ring clearance, % of normal value	Percent of values at shutoff with normal ring clearance			Percent of values at best efficiency with normal ring clearance		
			Q	H	P	η	H_0	P_0
2100 (0.77)	63 (19.2)	178	100	98.3	98.9	99.4	97.0	100
. . .	. . .	356	100	97.5	99.0	98.5	93.6	98.2
. . .	. . .	688	100	96.0	98.9	97.1	91.2	94.8
. . .	. . .	1375	100	94.3	97.4	96.8	88.8	92.5
3500 (1.28)	65 (19.8)	354	100	90.0	99.1	90.8	85.0	96.2
4300 (1.57)	41(12.5)	7270	62	65.5	81.7	49.8	44.3	106
4800 (1.76)	26 (7.9)	5220	96	78.8	89.2	84.8	78.2	83.3

Source: Flowserve Corporation

falls off as the rings wear. Table 3 shows some of the effects of increasing the clearance of rings similar to Figure 12a.

The labyrinth construction shown in Figure 12b has been used to increase the leakage path without increasing the axial length of the rings. If the pressure differential across these rings is high enough, the pump shaft may take on lateral vibrations with relatively large amplitude and long period, which can cause serious damage. One remedy for these vibrations is to increase clearance 2 in Figure 12b relative to clearance 1, at the expense of an increased leakage flow. High-pressure breakdown through plain rings may cause vibration,[10] but this is not usually a serious problem. It is considered good practice to replace or repair wearing rings when the nominal clearance has doubled. The presence of abrasive solids in the liquid pumped may be expected to increase wearing-ring clearances rapidly.

VANE-TIP CLEARANCE Many impellers are made without an outer shroud and rely on close running clearances between the vane tips and the casing to hold leakage across the vane tips to a minimum. Although this construction usually is not used with pumps having specific speeds less than about 6000 (2.20), Wood et al.[11] have reported good results with semiopen impellers at 1800 (0.66) $\leq n_s \leq$ 4100 (1.50). It appears that both head and efficiency increase with decreasing tip clearance and are quite sensitive to rather small changes in clearance. Reducing the tip clearance from about 0.060 in (1.5 mm) to about 0.010 in (0.25 mm) may increase the efficiency by as much as 10%. Abrasive solids in the liquid pumped probably will increase tip clearances rapidly.

MODIFICATIONS TO IMPELLER AND CASING

Diameter Reduction To reduce cost, pump casings usually are designed to accommodate several different impellers. Also, a variety of operating requirements can be met by changing the outside diameter of a given radial impeller. Eq. 6 shows that the head should be proportional to $(nD)^2$ provided that the exit velocity triangles (Figure 2b) remain similar before and after cutting, with w_2 always parallel to itself as u_2 is reduced. This can be achieved if the impeller meridional exit area $A_{m,2}$ is the same before and after cutting—and if the flow angle $\beta_{f,2}$ (Figure 15, Section 2.1) also stays the same. [$\beta_{f,2}$ would stay the same if the blade angle β_2 (= $\beta_{b,2}$) does, the difference being due to slip velocity V_s that should also scale down with D.] For radial discharge impellers, area $A_{m,2}$ equals $\pi D b_2$ (minus blade and boundary layer blockage) and requires that b_2 increase as D decreases. This is typical of many impellers—as is constancy of β_2 over the cutting range—and, together with Eqs. 27–33 of Section 2.1, leads to the so-called "affinity laws" for predicting performance:

$$\frac{Q_1}{Q_2} = \frac{n_1 D_1}{n_2 D_2} \tag{12a}$$

$$\frac{H_1}{H_2} = \frac{n_1^2 D_1^2}{n_2^2 D_2^2} \tag{12b}$$

$$\frac{P_1}{P_2} = \frac{n_1^3 D_1^3}{n_2^3 D_2^3} \tag{12c}$$

which apply only to a given impeller with altered D and constant efficiency but *not* to a geometrically similar series of impellers. The assumptions on which Eqs. 12 were based are rarely if ever fulfilled in practice, so exact predictions by the equations should not be expected. A common example is the low-n_s radial discharge impeller with parallel radial hub and shroud profiles over most of the path from inlet to exit (Figure 6). Here, $A_{m,2}$ decreases with cutting, and H falls more than would be predicted by Eq. 12b. [This type of impeller is often found in multistage pumps, particularly those in which the designer, driven by cost reduction goals, has minimized a) the axial length occupied by each stage and b) the number of stages, thereby pushing down the n_s of the individual stage to the point that a tolerable sacrifice in efficiency results.]

RADIAL DISCHARGE IMPELLERS Impellers of low specific speed may be cut successfully provided the following items are kept in mind:

1. The angle β_2 may change as D is reduced, but this usually can be corrected by filing the blade tips. (See the discussion on blade-tip filing that follows.)
2. Tapered blade tips will be thickened by cutting and should be filed to restore the original shape. (See the discussion below on blade-tip filing.)
3. Bearing and stuffing box friction remain constant, but disk friction should decrease with decreasing D.
4. The length of flow path in the pump casing is increased by decreasing D.
5. Because c_{m1} is smaller at the reduced capacity, the inlet triangles no longer remain similar before and after cutting, and local flow separation may take place near the blade entrance tips.
6. The second right-hand term in Eq. 5 was neglected in arriving at Eqs. 12, but it may represent a significant decrease in head as D is reduced.
7. Some blade overlap should be maintained after cutting. Usually the initial blade overlap decreases with increasing specific speed, so the higher the specific speed, the less the allowable diameter reduction.
8. Diameter reductions greater than from 10 to 20% of the original full diameter of the impeller are rarely made.

Most of the losses are approximately proportional to Q^2, and hence to D^2 by Eq. 12. Because the power output decreases approximately as D^3, it is reasonable to expect the maximum efficiency to decrease as the wheel is cut, and this often is the case. By Eq. 12 and the n_s-definition (Eq. 38a of Section 2.1), the product n_sD should remain constant so the specific speed at best efficiency increases as the wheel diameter is reduced (Table 4).

The characteristics of the pump shown in Figure 13 may be used to illustrate reduction of diameter at constant speed. Starting with the best efficiency point and $D = 16\frac{5}{16}$ in (41.4 cm), let it be required to reduce the head from $H = 224.4$ to $H' = 192.9$ ft (68.4 m to 58.8 m) and to determine the wheel diameter, capacity, and power for the new conditions.

Because the speed is constant, Eqs. 12 may be written

$$H = k_H Q^2 \quad and \quad P = k_p Q^3 \tag{13}$$

where k_H and k_p may be obtained from the known operating conditions at $D = 16\frac{5}{16}$ in (41.4 cm). Plot a few points for assumed capacities and draw the curve segments as shown by the solid lines in Figures 13*b* and 13*c*. Then, from Eqs. 12

$$D' = D\sqrt{H'/H} \qquad Q' = Q\sqrt{H'/H} \qquad P' = P(H'/H)^{3/2} \tag{14a}$$

$$D' = D(Q'/Q) \qquad H' = H(Q'/Q)^2 \qquad P' = P(Q'/Q)^3 \tag{14b}$$

from which $D = 15\frac{1}{8}$ in (38.4 cm), $Q = 3709$ gpm (234 l/s), and $P' = 215.5$ hp (160.7 kW). In Figure 13, the initial conditions were at points A and the computed conditions after cutting at points B. The test curve for $D = 15\frac{1}{8}$ in (38.4 cm) shows the best efficiency point a at a lower flow rate than predicted by Eqs. 14, but the head curve satisfies the predicted values very closely. The power prediction was not quite as good. Table 4 and Figure 13 give actual and predicted performance for three impeller diameters. The error in predicting the best efficiency point was computed by (predicted value minus test value) (100)/(test value). As the wheel diameter was reduced, the best efficiency point moved to a lower flow rate than predicted by Eq. 14 and the specific speed increased, showing that the conditions for Eqs. 12 to hold were not maintained.

Wheel cutting should be done in two or more steps with a test after each cut to avoid too large a reduction in diameter. Figure 14 shows an approximate correction, given by Stepanoff,[12] that may be applied to the ratio D'/D *as* computed by Eqs. 12 or 14. The accuracy of the correction decreases with increasing specific speed. Figure 15 shows a correction proposed by Rütschi[13] on the basis of extensive tests on low-specific-speed pumps. The corrected diameter reduction ΔD is the diameter reduction $D - D'$ given by Eqs. 14 and multiplied by k from Figure 15. The shaded area in Figure 15 indicates the range of scatter of the test points operating at or near maximum efficiency. Near shutoff the values of k were smaller and at maximum flow rate the values of k were larger than shown in Figure 15. Table 5 shows the results of applying Figures 14 and 15 to the pump of the preceding example.

There is no independent control of Q and H in impeller cutting, although Q may be increased somewhat by underfiling the blade tips as described later. The flow rate and power will automatically adjust to the values at which the pump head satisfies the system head-flow curve.

MIXED-FLOW IMPELLERS Diameter reduction of mixed-flow impellers is usually done by cutting a maximum at the outside diameter D_0 and little or nothing at the inside diameter D_i, as shown in Figure 16. Stepanoff[14] recommends that the calculations be based on the average diameter $D_{av} = (D_i + D_0)/2$ or estimated from the blade-length ratio *FK*/*EK* or *GK*/*EK* in Figure 16d. Figure 16 shows a portion of the characteristics of a mixed-flow impeller on which two cuts were made as in Figure 16b. The calculations were made by Eqs. 14 using the mean diameter

$$D_m = \sqrt{(D_o^2 + D_i^2)/2}$$

instead of the outside diameter in each case. The predictions and test results are shown in Figure 16 and Table 6. It is clear that the actual change in the characteristics far exceeded

TABLE 4 Predicted characteristics at different impeller diameters on a radial-flow pump

	Test values					Predicted from D = $16\frac{5}{16}$ in (41.4 cm)			Predicted from D = $15\frac{1}{8}$ in (88.4 cm)		
D, in (cm)	Q, gpm (l/s)	H, ft (m)	P, hp (kW)	n_s (Ω_s)	n_sD (Ω_sD)	Q', gpm (l/s)	H', ft (m)	P', hp (kW)	Q', gpm (l/s)	H' ft (m)	P', hp (kW)
$16\frac{5}{16}$ (41.4)	4000 (252)	224.4 (68.4)	270.4 (201.6)	1953 (0.7146)	31,860 (29.54)	. . .	. . .	. . .	3888 (245) −2.93% error[a]	227.3 (69.3) 1.29% error[a]	272.2 (203.0) 0.68% error[a]
$15\frac{1}{8}$ (38.4)	3600 (227.1)	195.4 (59.6)	217.0 (161.8)	2055 (0.7519)	31,080 (28.87)	3709 (234) 3.02% error[a]	192.9 (58.8) −1.28% error[a]	215.5 (160.7) −0.69% error[a]	. . .	. . .	. . .
14 (35.6)	3200 (201.9)	163.6 (49.9)	167.2 (124.7)	2214 (0.8101)	31,000 (28.84)	3433 (217) 7.28% error[a]	165.3 (50.4) 1.03% error[a]	170.9 (127.4) 2.33% error[a]	3332 (210.2) 4.13% error[a]	167.4 (51.0) 2.33% error[a]	172.1 (128.3) 2.93% error[a]

[a]Error in predicting best efficiency point.

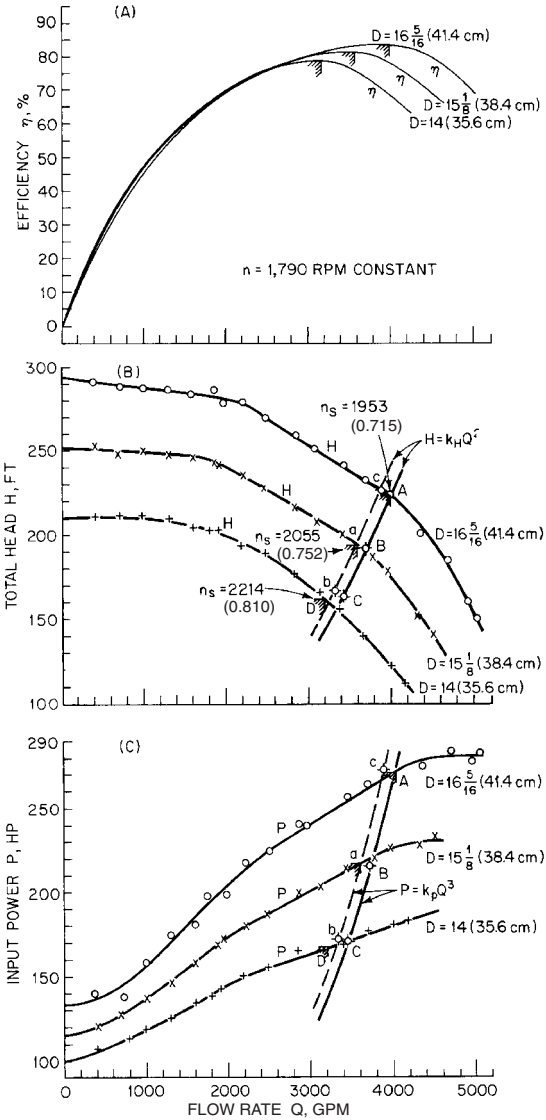

FIGURE 13A through C Diameter reduction of radial-flow impeller (gpm × 0.06309 = l/s). D is measured in inches (centimeters).

the predicted values. Except for the use of the mean diameters, the procedure was essentially the same as that described for Figure 13, and all points and curves are similarly labeled. The corrections given in Figure 14 would have made very little difference in the computed diameter reductions, and those of Figure 15 were not applicable to impellers having specific speeds greater than $n_s = 2000$ (0.73). In this case, the product $n_s D_m$ did not remain constant and the maximum efficiency increased as D_m was reduced. Although the

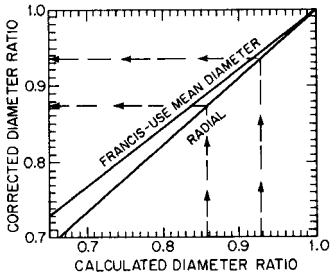

FIGURE 14 Corrections for calculated impeller diameter reductions (Reference 12)

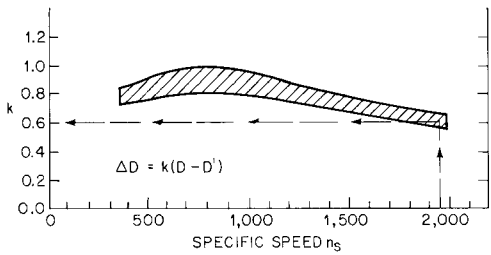

FIGURE 15 Corrections for calculated impeller diameter reductions (Reference 13). ($\Omega_s = n_s/2733$)

TABLE 5 Impeller diameter corrections

D before cutting	in	16.3125	16.3125
D' predicted by Eqs. (14)	in	15.125	14.000
D' corrected by Figure 14	in	15.25[a]	14.26[b]
D' corrected by Figure 15	in	15.60[c]	14.93[d]

[a] D'/D = 15.125/16.3125 = 0.927; by Figure 14, corrected D'/D = 0.935. Corrected D' = (0.935)(16.3125) = 15.25 in.

[b] D'/D = 14.000/16.3125 = 0858; by Figure 14, corrected D'/D = 0.874. Corrected D' = (0.874)(16.3125) = 14.26 in.

[c] $D - D'$ = 16.3125—15.125 = 1.1875; by Figure 15, $K \cong 0.6$ at n_s = 1,953. Corrected $D - D'$ = (0.6)(1.1875) = 0.7125 and corrected D' = 16.3125—0.7125 = 15.60 in.

[d] $D - D'$ = 16.3125—14.000 = 2.3125; by Figure 15, $K \cong 0.6$ at n_s = 1,953. Corrected $D - D'$ = (0.6)(2.3125) = 1.3875 and corrected D' = 16.3125—1.3875 = 14.93 in.

changes in diameter were small, the area of blade removed was rather large for each cut. The second cut eliminated most of the blade overlap.

The characteristics of mixed-flow impellers can be changed by cutting, but very small cuts may produce a significant effect. The impellers of propeller pumps are not usually subject to diameter reduction.

Shaping Blade Tips If the discharge tips of the impeller blades are thick, performance usually can be improved by filing over a sufficient length of blade to produce a long, gradual taper. Chamfering, or rounding, the discharge tips may increase the losses and should never be done. Reducing the impeller diameter frequently increases the tip thickness.

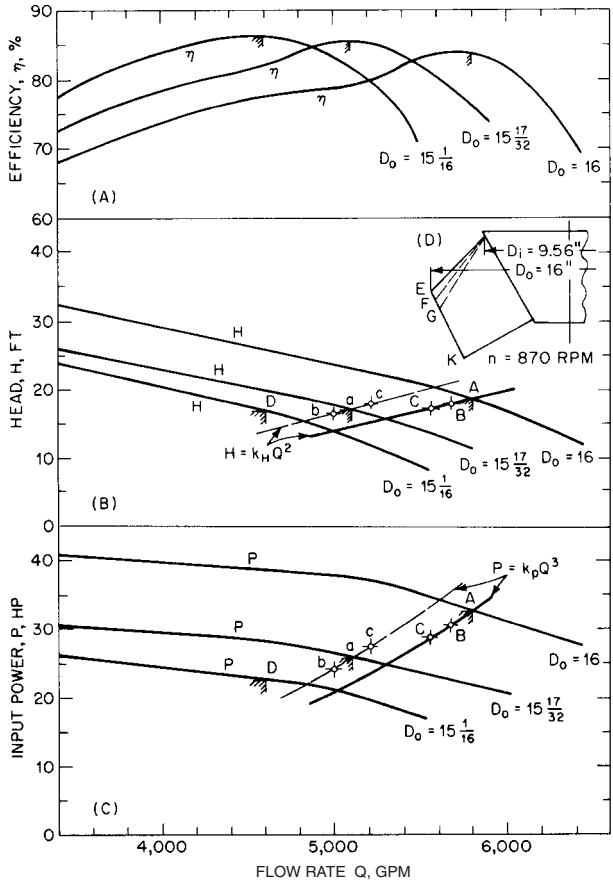

FIGURE 16A through C Diameter reduction of mixed-flow impeller (ft × 0.3048 = m; in × 2.540 = cm; gpm × 0.06309 = l/s; hp × 0.7457 = kW)

OVERFILING This is shown at *B* in Figure 17, and the unfiled blade is shown at *A*. Usually there is little or no increase in the blade spacing d before and d_F after filing, so the discharge area is practically unchanged. Experience indicates that any change in the angle β_2 due to overfiling usually produces a negligible change in performance.

UNDERFILING This is shown at C in Figure 17. If properly done, underfiling will increase the blade spacing from d to d_f and hence the discharge area, which lowers the average meridional velocity c_{m2}, at any given flow rate Q. The angle β_2 usually is increased slightly. Figure 18*A* and Eq. 6 show that the head and consequently the power increase at the same flow rate. The maximum efficiency usually is improved and may be moved to a higher flow rate. At the same head, Figure 18*B* shows that both c_{m2} and the flow rate will increase. The change both in the area and in C_{m2} may increase the flow rate by as much as 10%. Table 7 shows the results of tests before and after underfiling the impeller blades of nine different pumps. In general, they confirm the foregoing predictions based on changes in area and in the velocity triangles.

TABLE 6 Predicted characteristics at different impeller diameters on a mixed-flow pump

		Test values					Predicted from D = 16.00 (40.64 cm), D_m = 13.17 (33.45 cm)			Predicted from D = 15.53 (39.45 cm), D_m = 12.89 (32.74 cm)		
D, in (cm)	D_m, in (cm)	Q, gpm (l/s)	H, ft (m)	P, hp (kW)	n_s	n_sD_m	Q', gpm (l/s)	H', ft (m)	P', hp (kW)	Q', gpm (l/s)	H', ft (m)	P', bp (kW)
16 (40.64)	13.17 (33.45)	5800 (365.9)	18.6 (5.67)	32.5 (24.2)	7385 (2.702)	97,300 (90.39)	. . .	. . .	. . .	5210 (329) −11.3% error	17.9 (5.46) −3.91% error	27.4 (20.4) −18.6% error
$15\frac{17}{32}$ (39.45)	12.89 (32.74)	5100 (321.8)	17.1 (5.21)	25.7 (19.2)	7385 (2.702)	95,200 (88.47)	5680 (358.4) 10.2% error[a]	17.8 (5.43) 4.50% error[a]	30.4 (22.7) 15.5% error[a]			
$15\frac{1}{16}$ (38.26)	12.62 (32.05)	4600 (290.2)	16.8 (5.12)	22.6 (17.1)	7100 (2.598)	89,600 (83.26)	5560 (350.8) 17.3% error[a]	17.1 (5.21) 1.75% error[a]	28.6 (21.6) 21.0% error[a]	5000 (315.5) 8.00% error[a]	16.4 (5.00) −2.44% error[a]	24.1 (18.2) 6.22% error[a]

[a]Error in predicting best efficiency point.

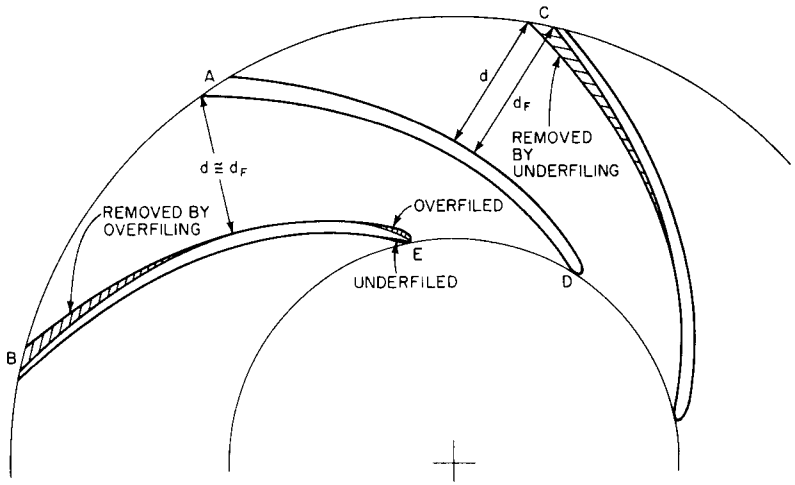

FIGURE 17 Underfiling and overfiling of blade tips

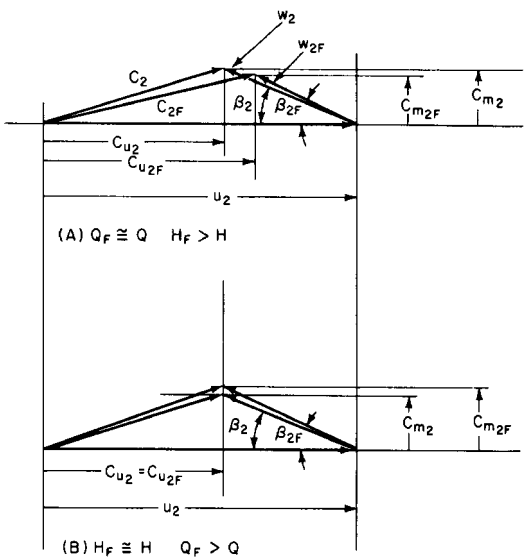

FIGURE 18 Discharge velocity triangles for underfiled blades (neglecting slip)

INLET BLADE TIPS If the inlet blade tips are blunt, as shown at D in Figure 17, the cavitation characteristics may be improved by sharpening them, as shown at E. In this case overfiling increases the effective flow area, which reduces c_{m1} for a given flow rate. If more area is needed, it may be advantageous to cut back part of the blade and sharpen the leading edge. Overfiling tends to increase β_1, which is incompatible with a decrease in c_{m1} (Figure 19). The increase in β_1 increases the angle of attack of the liquid approaching the blade. In Figures 2 and 19, w_1 is tangent to the centerline of the blade at entrance and w_0

TABLE 7 Changes in performance when impeller blades are underfiled

Specific speed n_s	Ω_s	No. of stages	Impeller diameter D_2, in	(cm)	Change in blade spacing d_F/d	$\frac{H_F - H}{H}$ %[b]	Changes at best efficiency point after filing, % H_o[c]	H	Q	P	η
862	(0.3154)	1	$11\frac{1}{2}$	(29.21)	1.13	4	1.5	4	0	9	−5
945	(0.3458)	2	$8\frac{3}{8}$	(21.27)	1.05	5.5	0	3	4	−0.5	7.5[d]
1000	(0.3659)	4	$9\frac{1}{8}$	(23.18)	1.055	5.5	0	5.5	0	3	2.5
1080	(0.3952)	2	$9\frac{13}{16}$	(24.92)	1.08	10	2.5	10	0	6.8	3
1525	(0.5580)	2	$10\frac{1}{2}$	(26.67)	1.035	3.2	3	0.5	4.5	3.5	1.2
1950	(0.7135)	1	22	(55.88)	1.02	1.5	1	1.5	0	1.5	0
3300[a]	(1.2075)	1	12	(30.48)	. . .	7.8	2.5	7.8	0	8.5	−0.6
3450[a]	(1.2623)	1	$30\frac{1}{2}$	(77.47)	. . .	6.5	0.5	6.5	0	7.8	−2.2
4300	(1.5734)	1	$41\frac{1}{4}$	(104.8)	. . .	5		5	0	0.5	4.5[e]

[a]Double suction.
[b]H_F is head after filing.
[c]Shutoff head.
[d]Due in part to changes in pump casing.
[e]Due in part to rounding of inlet blade tips.
Source: Flowserve Corporation

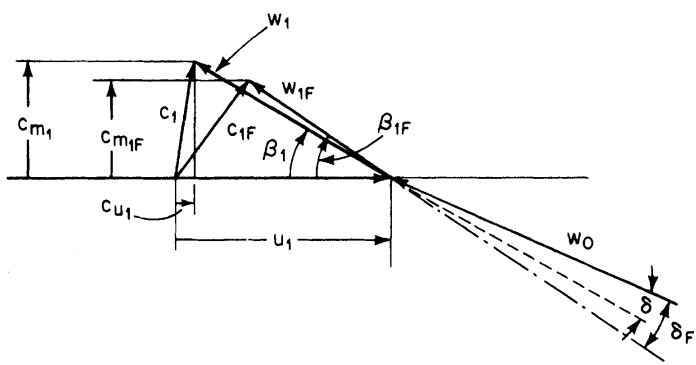

FIGURE 19 Effect of overfiling at inlet on the velocity triangle just inside the blades

is the velocity of the approaching liquid as seen by an observer moving with the blade. The angle δ between w_0 and w_1 is the angle of attack, which increases to δ_F after overfiling. Although the increase in δ tends to increase the opportunity for the liquid to separate from the low-pressure face of the blade, this disadvantage usually is outweighed by the improvement that results when c_{m1} is reduced.*

*The distinction between a true velocity diagram formed just upstream of the impeller blades and the triangles shown just inside the blades in Figure 19 should be noted. w_1 in this figure is shown aligned with the blade, having undergone an adjustment in direction via incidence from that of the approaching w_0. Only by plotting the velocity diagram just upstream of this point can one determine the true value of the circumferential component c_{u1} of the absolute velocity being delivered to the impeller by the upstream piping, vanes, and so on. It is this delivered value of c_{u1} that must be used in computing input or ideal head of the impeller (Eq. 15b, Section 2.1 or, neglecting slip, Eq. 6 of this subsection). Thus w_0 is properly the true w_1 vector and should be understood as such (see Section 2.1).

CASING TONGUE The casing tongue or cutwater forms part of the throat of the discharge nozzle of many volute casings (Figure 20a, Section 2.1). Frequently the throat area is small enough to act as a throttle and reduce the maximum flow rate otherwise obtainable from the impeller. Cutting back the tongue increases the throat area and increases the maximum flow rate. The head-versus-flow rate characteristic is then said to *carry out farther.* Shortening the discharge nozzle may increase the diffusion losses a little and result in a slightly lower efficiency.

CAVITATION

The formation and subsequent collapse of vapor-filled cavities in a liquid due to dynamic action are called *cavitation.* The cavities may be bubbles, vapor-filled pockets, or a combination of both. The local pressure must be at or below the vapor pressure of the liquid for cavitation to begin, and the cavities must encounter a region of pressure higher than the vapor pressure in order to collapse. Dissolved gases often are liberated shortly before vaporization begins. This may be an indication of impending cavitation, but true cavitation requires vaporization of the liquid. Boiling accomplished by the addition of heat or the reduction of static pressure without dynamic action of the liquid is arbitrarily excluded from the definition of cavitation.

When a liquid flows over a surface having convex curvature, the pressure near the surface is lowered and the flow tends to separate from the surface. *Separation* and *cavitation* are completely different phenomena. Without cavitation, a separated region contains turbulent eddying liquid at pressures higher than the vapor pressure. When the pressure is low enough, the separated region may contain a vapor pocket that fills from the downstream end,[15] collapses, and forms again many times each second. This causes noise and, if severe enough, vibration. Vapor-filled bubbles usually are present and collapse very rapidly in any region where the pressure is above the vapor pressure. Knapp[16] found the life cycle of a bubble to be on the order of 0.003 s.

Bubbles that collapse on a solid boundary may cause severe mechanical damage. Shutler and Mesler[17] photographed bubbles that distorted into toroidal-shaped rings during collapse and produced ring-shaped indentations in a soft metal boundary. The bubbles rebounded following the initial collapse and caused pitting of the boundary. Pressures on the order of 10^4 atm have been estimated[18] during collapse of a bubble. All known materials can be damaged by exposure to bubble collapse for a sufficiently long time. This is properly called *cavitation erosion,* or *pitting.* Figure 20 shows extensive damage to the suction side of pump impeller vanes after about three months' operation with cavitation. At two locations, the pitting has penetrated deeply into the $\frac{3}{8}$-in (9.5-mm) thickness of stainless steel. The unfavorable inlet flow conditions, believed to have been the cause of the cavitation, were at least partly due to elbows in the approach piping. Modifications in the approach piping and the pump inlet passages reduced the cavitation enough to extend impeller life to several years.[19]

It has been postulated that high temperatures and chemical action may be present at bubble collapse, but any damaging effects due to them appear to be secondary to the mechanical action. It seems possible that erosion by foreign materials in the liquid and cavitation pitting may augment each other. Controlled experiments[20] with water indicated that the damage to metal depends on the liquid temperature and was a maximum at about 100 to 120°F (38 to 49°C). Cavitation pitting, as measured by weight of the boundary material removed per unit time, frequently increases with time. Cast iron and steel boundaries are particularly vulnerable. Controlled experiments have shown that cavitation pitting in metals such as aluminum, steel, and stainless steel depends strongly on the velocity of the fluid in the undisturbed flow past the boundary. On the basis of tests of short duration, Knapp[15] reported that damage to annealed aluminum increased approximately as the sixth power of the velocity of the undisturbed flow past the surface. Hammitt[21] found a more complicated relationship between velocity and damage, as shown in Figure 21. It seems clear that after cavitation begins, it will increase rapidly with increasing velocities. Frequently the rate of pitting accelerates with elapsed time. Comprehensive discussions of cavitation and erosion together with additional references are given by Preece.[22]

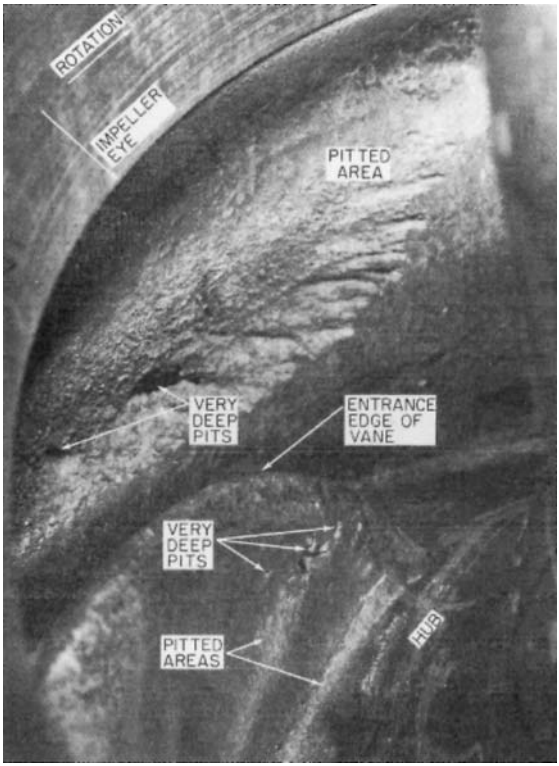

FIGURE 20 Impeller damaged by cavitation (Demag Delaval, Reference 19)

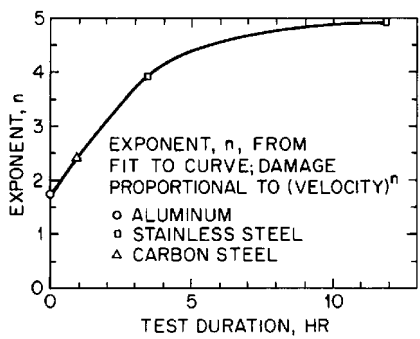

FIGURE 21 Cavitation damage exponent versus test time for several materials in water (Reference 21)

Centrifugal pumps begin to cavitate when the suction head is insufficient to maintain pressures above the vapor pressure throughout the flow passages. The most sensitive areas usually are the low-pressure sides of the impeller vanes near the inlet edge and the front shroud, where the curvature is greatest. Axial-flow and high-specific-speed impellers without front shrouds are especially sensitive to cavitation on the low-pressure

sides of the vane tips and in the close tip-clearance spaces. Sensitive areas in the pump casing include the low-pressure side of the tongue and the low-pressure sides of diffusion vanes near the inlet edges. As the suction head is reduced, all existing areas of cavitation tend to increase and additional areas may develop. Apart from the noise and vibration, cavitation damage may render an impeller useless in as little as a few weeks of continuous operation. In multistage pumps cavitation usually is limited to the first stage, but Kovats[23] has pointed out that second and higher stages may cavitate if the flow is reduced by lowering the suction head (submergence control). Cavitation tends to lower the axial thrust of an impeller. This could impair the balancing of multistage pumps with opposed impellers. A reduction in suction pressure may cause the flow past a balancing drum or disk to cavitate where the liquid discharges from the narrow clearance space. This may produce vibration and damage resulting from contact between fixed and running surfaces.

Net Positive Suction Head (NPSH) Several criteria exist for establishing the *NPSH* of a pump. These are connected with a) inception of cavitation, b) loss of hydraulic performance, and c) protecting the pump against cavitation erosion or damage. These are defined and found as follows:

a. *Inception NPSH*. Cavitation can be completely prevented so long as the static pressure within the pump is everywhere greater than the vapor pressure of the liquid. This can be achieved if the *NPSH* (also called h_{su}), defined in Section 2.1 as the total head of the pumped liquid at the pump inlet datum or suction flange above that vapor pressure, is sufficiently large. The value of *NPSH* that achieves this is called $NPSH_i$, namely, the "inception *NPSH*."

b. *Performance NPSH*. In a typical *NPSH*-test at constant speed n and flow rate Q, a substantial reduction of *NPSH* below $NPSH_i$ is usually necessary to reach the value that produces an identifiable drop in performance—usually 3% of pump stage total pressure rise or pump head. This value is called the "required *NPSH*," *NPSHR* or $NPSH_{3\%}$. Table 1 in Section 2.1 provides empirical correlations for $NPSH_{3\%}$ for common pumps and inducers. Other criteria for $NPSH_{3\%}$ will be given further on. The domains of cavitation within a pump are widespread at this condition, and experience shows that a head drop in the neighborhood of 3% must occur in order to obtain a repeatable value of *NPSHR* on test[12]. Lower percentages have been demanded by users, but they invariably give rise to a large scatter in the measured *NPSHR* for even small variations in any of the test variables.

It used to be thought throughout the pump community that there are no cavities or bubbles present at zero percent head drop due to cavitation activity within a pump. In recent decades, however, it has been proven through many observations that not only is the head drop equal to zero at inception (where $NPSH = NPSH_i$), it remains so for an enormous range of lesser NPSH-values over which extensive bubble activity is observed. In fact, $NPSH_i$ is commonly from two to five times the magnitude of the *NPSHR* that is associated with any noticeable drop in pump head. At the 3% (or lesser percentage) head drop condition, actual observations of the cavitating flow show the cavities to extend all the way from the leading edge of each blade to the throat formed by the leading edge of the next blade[24]. In the face of these learnings, it is evident that to demand a test for the NPSH required for a head drop of much less than 3% usually causes only needless misunderstandings and expenditure of time and money.

c. *Damage-Limiting NPSH or Life NPSH*. If it is desired to substantially reduce or eliminate cavitation activity within the pump, an acceptance test should be conducted wherein the cavitating flow can be observed visually[25]. This is indeed a serious issue if the pump energy level is high enough (and therefore the inlet pressure) for the collapsing cavities to do damage (as in Figure 20; see also Section 2.1). In such a case, "$NPSH_{3\%}$" has virtually no meaning; rather, the truly *required NPSH* or "*NPSHR*" is that *larger* value which satisfactorily limits the extent of this visually observed cavitation within the pump or pump model[26].

Therefore, the *available NPSH* at the installation must be at least equal to the *required NPSH* if the above consequences are to be avoided—be they significant loss of

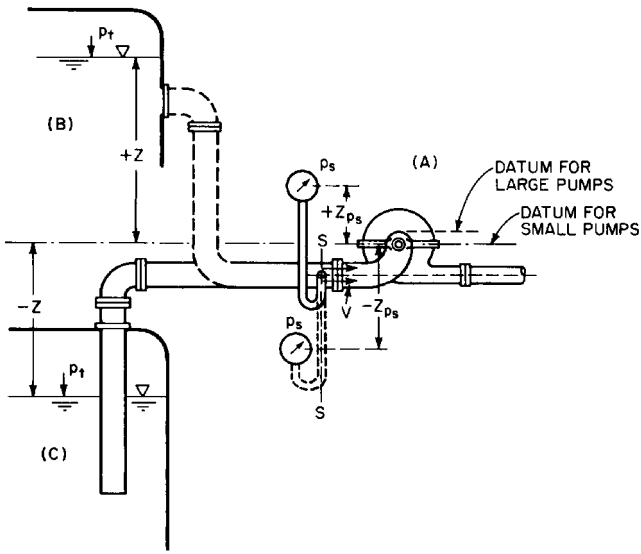

FIGURE 22 Definition sketch for computing NPSH

pump head (that is, loss of hydraulic performance) or damage due to collapsing cavities. Increasing the available *NPSH* above the required value provides a margin of safety against unpredictable variations of conditions, including transient behavior. Figure 22 and the following symbols will be used to compute the available *NPSH*:

p_a = absolute pressure in atmosphere surrounding gage, Figure 22

p_s = gage pressure indicated by gage or manometer connected to pump suction at section *s-s;* may be positive or negative

p_t = absolute pressure on free surface of liquid in closed tank connected to pump suction

p_{vp} = vapor pressure of liquid being pumped corresponding to the temperature at section *s-s* (if liquid is a mixture of hydrocarbons, p_{vp} must be measured by the *bubble point* method)

h_f = lost head due to friction in suction line between tank and section *s-s*

V = average velocity at section *s-s*

Z, Z_{ps} = vertical distances defined by Figure 22; may be positive or negative

γ = specific weight of liquid at pumping temperature

It is satisfactory to choose the datum for small pumps as shown in Figures 1 and 22, but with large pumps, the datum should be raised to the elevation where cavitation is most likely to start. For example, the datum for a large horizontal-shaft propeller pump should be taken at the highest elevation of the impeller-blade tips. The available *NPSH* is given by

$$h_{sv} = \frac{p_a - p_{vp}}{\gamma} + \frac{p_s}{\gamma} + Z_{ps} + \frac{V^2}{2g} \tag{15}$$

or

$$h_{sv} = \frac{p_t - p_{vp}}{\gamma} + Z - h_f \tag{16}$$

Consistent units must be chosen so that each term in Eqs. 15 and 16 represents feet (or meters) of the liquid pumped. Equation 15 is useful for evaluating the results of tests. Equation 16 is useful for estimating available *NPSH* during the design phase of an installation. In Eq. 15, the first term represents the height of a liquid barometer, h_b, containing the liquid being pumped and the sum of the remaining terms represents the suction head h_s; that is, the total head H (Eq. 3, Section 2.1) evaluated at the suction flange S in Figure 22. Therefore

$$h_{sv} = h_b + h_s \tag{17}$$

Usually, a positive value of h_s is called a *suction head* and a negative value of h_s is called a *suction lift*.

Many pumps draw cold water from reservoirs exposed to atmospheric pressure, so the suction lift is limited if there is to be a reasonable value of h_{sv} (= *NPSH*) available at the pump suction flange or port. In normal practice, rather small values of suction lift or suction head are encountered in many installations, so one can depend on the value of h_{sv} being a substantial portion of h_b—say about 60% or 20 ft (6m) of water column. Recognizing that the suction specific speed capability S of most pumps falls within a rather small range has led to charts of recommended operating speeds such as those in Section 9.10 or the speed recommendations of Figure 23 for condensate pumps for varying amounts of *NPSH* available. In fact, $S = 8500$ ($\Omega_{ss} = 3.11$) is recommended by the Hydraulic Institute[27]. S (= N_{ss}) and Ω_{ss} are defined in Eqs. 41 and 42 of Section 2.1. The relationship of suction-specific speed to other suction parameters is treated further on.

Cavitation Tests In addition to the constant-Q tests for *NPSHR* that were described in the foregoing review of the various *NPSH*-criteria, one can establish the curve of performance *NPSH* versus flow rate by varying the *NPSH* available and seeing how much flow

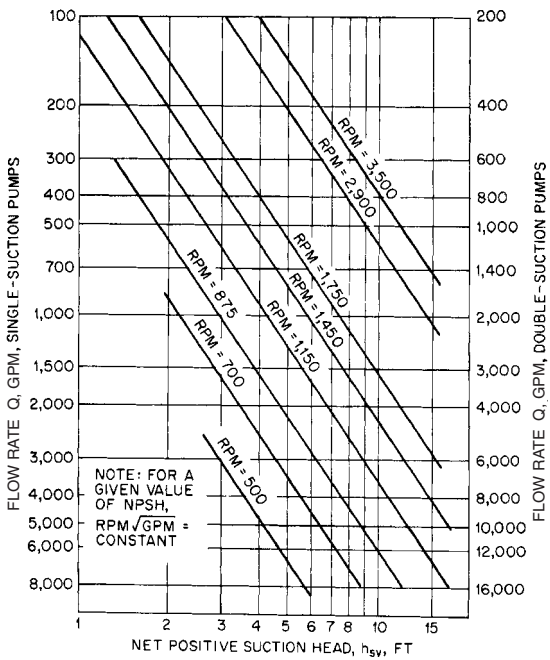

FIGURE 23 Capacity (flow rate) and speed limitations for condensate pumps with shaft through eye of impeller (ft × 0.3048 − m; gpm × 0.06309 = l/s) (adapted from Hydraulic Institute ANSI/HI 2000 Edition Pump Standards, Reference 27)

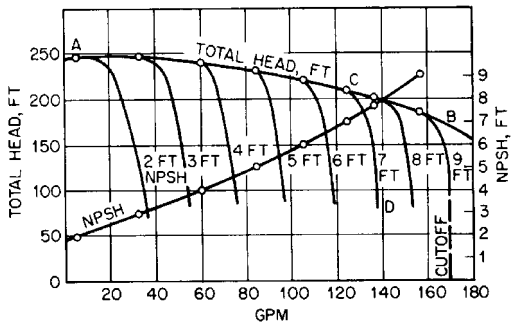

FIGURE 24 Test of a 1.5-in (3.81-cm) single-stage pump at 3470 rpm, on water, 70°F (2l°C) (ft × 0.3048 = m; gpm × 0.06309 = l/s) (Reference 12)

rate Q the pump can handle. This is illustrated in Figure 24, wherein a different head curve is found for each value of *NPSH*. For each such curve, as Q is increased, there is a point at which the head departs from the next one of higher *NPSH*. This, then, is the Q for which the given *NPSH* is that required to maintain head, essentially $NPSH_{3\%}$. At higher flow rate, performance is lost, each head curve possessing a "cutoff" flow rate. References 27 and 28 may be consulted for details of test procedures.

Thoma Cavitation Parameter σ All the terms in Eqs. 15 to 17 may be made dimensionless by dividing each by the pump head H. The resulting parameter

$$\sigma = \frac{h_{sv}}{H} \tag{18}$$

has proven to be useful especially for high-specific speed pumps and turbines. The loading on the blades of a variable-pitch propeller, and therefore the minimum suction-side static pressure, is directly connected to the head developed. As this head increases with increasing blade setting angle, the loading increases, the minimum pressure drops, and the *NPSHR* goes up. Hence an identifiable limiting value of σ is found to exist for such a machine. σ-limits are presented for a range of specific speeds in Figure 25.

Performance-*NPSH* data are sometimes given in terms of σ; for example, Rütschi[13] presents the effect of pump hydraulic efficiency on *NPSH* in these terms, a consistently higher value of σ being required for pumps with lower efficiency (Figure 26).

Suction-Specific Speed For pumps in which the eye diameter of the impeller is smaller than that at exit, the pressures on the suction-sides of the blades that are associated with most of the head addition are in a region of higher pressure than in the vicinity of the eye. Thus Wislicenus[29] was able to decouple the eye from outer diameter of the pump (where most of the head is generated in a radial-flow machine) and show that only the eye geometry determines performance-*NPSH* and not the magnitude of the head created by the impeller. He demonstrated that for most centrifugal pumps (except the propellers just described), there is a small range of suction specific speed—from which the performance-*NPSH* can be determined. As in defined in Section 2.1, this parameter is defined as follows:

$$S = \frac{N\sqrt{Q}}{(h_{sv})^{3/4}} \tag{19}$$

Note that Q = *half the discharge* of a double-suction impeller when computing S. Equations 18 and 19 and the definition of n_s may be combined to yield

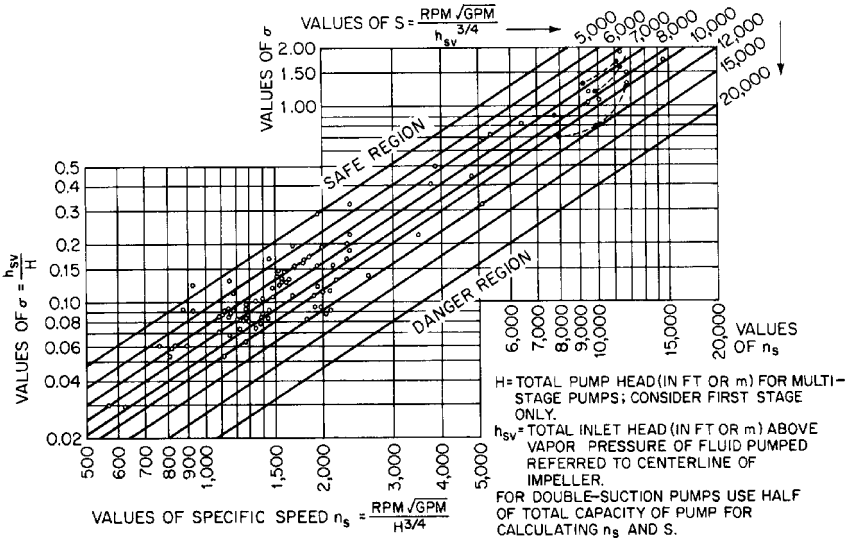

FIGURE 25 Cavitation limits of centrifugal and propeller pumps (Flowserve Corporation)

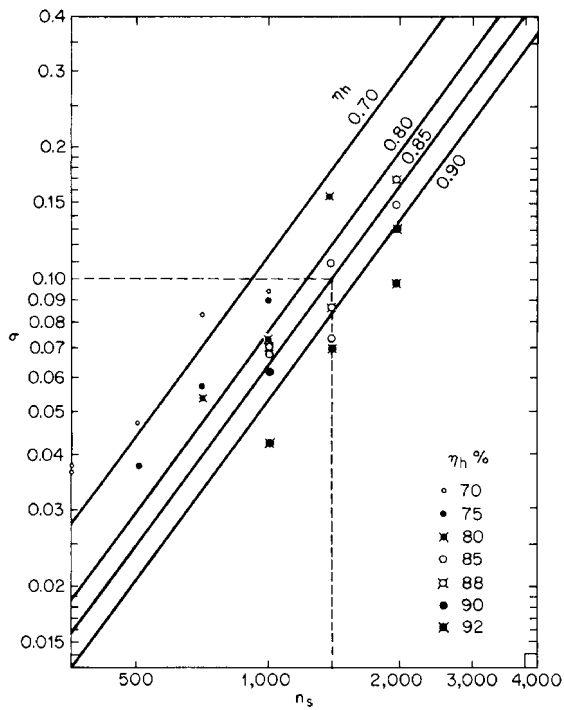

FIGURE 26 Cavitation parameter σ versus specific speed for different efficiencies ($\Omega_s = n_s/2733$) (Reference 13)

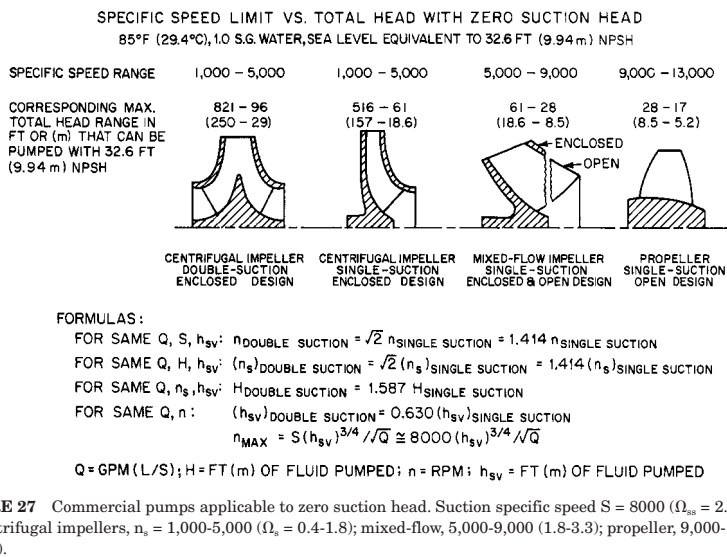

FIGURE 27 Commercial pumps applicable to zero suction head. Suction specific speed S = 8000 (Ω_{ss} = 2.93). For centrifugal impellers, n_s = 1,000-5,000 (Ω_s = 0.4-1.8); mixed-flow, 5,000-9,000 (1.8-3.3); propeller, 9,000-13,000 (1.3-4.8).

$$\sigma = \left(\frac{n_s}{S}\right)^{4/3} \tag{20}$$

$$n_s = S(\sigma)^{3/4} \tag{21}$$

Figure 25 shows lines of constant S. For most pumps, $7500 < S < 11{,}000$ ($2.7 < \Omega_{SS} < 4.0$), S = 8500 (3.11) being recommended by the Hydraulic Institute ANSI/HI 2000 Pump Standards (Reference 27). Higher values may apply to special designs or service conditions, such as an inducer ahead of the first-stage impeller. For a given specific speed, the lower the value of S, the safer the pump against cavitation. Experience with large European pumped storage installations has shown that cavitation effects began at $S \approx 6000$ (2.2), and this value is recommended for large pumps. Figure 27 shows a summary of data and formulas that may be useful with commercial pumps.

German practice differs considerably from that in the United States in computing suction specific speed. Pfleiderer[1] defined a hub correction k as

$$k = 1 - \left(\frac{d_h}{D_o}\right)^2 \tag{22}$$

where d_h = the hub diameter and D_o = the diameter of the suction nozzle, in any consistent units. The suction specific speed S_G is defined as

$$S_G = \frac{(n/100)^2 Q}{k h_{sv}^{3/2}} \tag{23}$$

where n is measured in rpm, Q in cubic meters per second per impeller inlet, and h_{sv} in meters of liquid pumped. It follows that

$$S = 5164\sqrt{S_G k} \tag{24}$$

NPSH for Liquids Other Than Cold Water Field experience, together with carefully controlled laboratory experiments, has indicated that pumps handling hot water or cer-

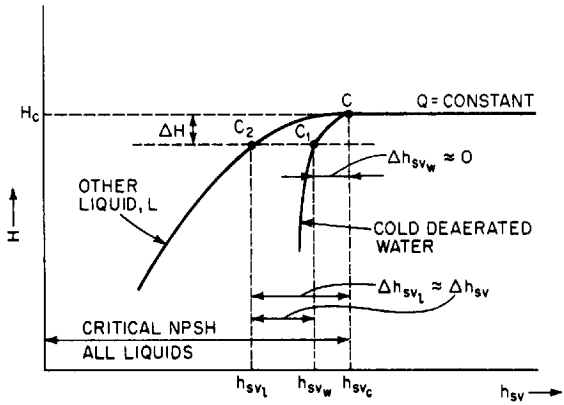

FIGURE 28 Cavitation tests with different liquids at constant speed and constant flow rate (Reference 34)

tain liquid hydrocarbons may be operated safely with less *NPSH* than would normally be required for cold water. This may lower the cost of an installation appreciably, particularly in the case of refinery pumps. A theory for this has been given by Stepanoff and others.[14,30–33] Figure 28 shows the results of cavitation tests on two liquids for constant capacity and constant pump speed. No head loss due to cavitation is present at point C or at $h_{sv} > h_{svc}$. With cold deaerated water, lowering h_{sv} slightly below h_{svc} produces limited cavitation and a decrease in pump head ΔH to point C_1, but Δh_{svw} usually is negligible. With hot water ($T \geq 100°F = 37.8°C$) or with many liquid hydrocarbons, a much larger decrease in h_{sv} will be required to produce the same drop in head ΔH that was shown by the cold water test. The *NPSH reduction,* or *NPSH adjustment,* is $\Delta H_{sv} \approx \Delta h_{svl.}$ In practice, ΔH has been limited *to* $\Delta h \leq 0.03H$, for which there is a negligible sacrifice in performance. The pumps usually are made of stainless steel or other cavitation-resistant materials, and the lower *NPSH* results in lower collapse pressure of the vapor bubbles, reducing the damage potential.

Chart for NPSH Reductions A composite chart of *NPSH reductions* for deaerated hot water and certain gas-free liquid hydrocarbons is shown in Figure 29. The curves of vapor pressure versus temperature and the curves of constant *NPSH* reduction were based on laboratory tests with the liquids shown and should be used subject to the following limitations:

1. No *NPSH* reduction should exceed 50% of the *NPSH* required by the pump for cold water or 10 ft (3.0 m), whichever is smaller.
2. *NPSH* may have to be increased *above* the normal cold-water value to avoid unsatisfactory operation when (*a*) *entrained* air or other noncondensable gas is present in the liquid or (*b*) *dissolved* air or other noncondensable gas is present in the liquid and the absolute suction pressure is low enough to permit release of the gas from solution.
3. The vapor pressure of hydrocarbon mixtures vary significantly with temperature and so should be determined at pumping temperature (see Reference 27).
4. If the suction system may be susceptible to transient changes in absolute pressure or temperature, a suitable margin of safety in *NPSH* should be provided. This is particularly important with hot water and may exceed the reduction that would otherwise apply with steady-state conditions.
5. Although experience has indicated the reliability of Figure 29 for hot water and the liquid hydrocarbons shown, its use with other liquids is not recommended unless it is clearly understood that the results must be accepted on an experimental basis.

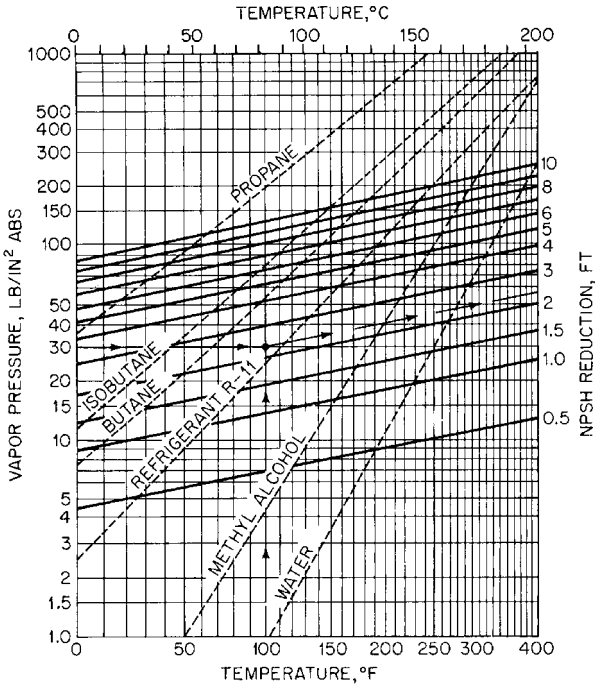

FIGURE 29 *NPSH* reductions for pumps handling liquid hydrocarbons and hot water. This chart has been constructed from test data obtained by using the liquids shown. For applicability to other liquids, refer to the text (ft × 0.3048 = m; lb/in² × 6.895 = kPa). (Hydraulic Institute ANSI/HI 2000 Edition Pump Standards, Reference 27)

USE OF FIGURE 29 Given a fluid having a vapor pressure of 30 lb/in² (210 kPa) abs at 100°F (37.8°C). Follow the arrows on the key shown on the chart and obtain an *NPSH* reduction of about 2.3 ft (0.70 m). Since this does not correspond to one of the liquids for which vapor pressure curves are shown on the chart, the use of this *NPSH* reduction should be considered a tentative value only. Given a pump requiring 16-ft (4.9-m) cold-water *NPSH* at the operating capacity, the pump is to handle propane at 55°F (12.8°C). Figure 29 shows the vapor pressure to be about 105 lb/in² (733 kPa) abs and the *NPSH* reduction to be about 9.5 ft (2.9 m). Since this exceeds 8 ft (2.44 m), which is half the cold-water *NPSH,* the recommended *NPSH* for the pump handling propane is half the cold-water *NPSH,* or 8 ft (2.44 m). If the temperature of the propane in the previous example is reduced to 14°F (−10°C), Figure 29 shows the vapor pressure to be 50 lb/in⁵ (349 kpa) abs and the *NPSH* reduction to be about 5.7 ft (1.74 m), which is less than half the coldwater *NPSH.* The *NPSH* required for pumping propane at 14°F (−10°C) is then 16 − 5.7 = 10.3 ≈ 10 ft (4.87 − 1.74 = 3.13 ≈ 3 m).

Reduction of Cavitation Damage After the pump has been built and installed*, there is little that can be done to reduce cavitation damage. As previously mentioned, sharpening the leading edges of the blades by filing may be beneficial. Stepanoff[12] has suggested cutting back part of the blades in the impeller eye together with sharpening the tips, for low-specific-speed pumps, as a means of reducing the inlet velocity c_1 and thus lowering σ. Although a small amount of prerotation or prewhirl in the direction of impeller rota-

*Sometimes it is possible to lower the pump, and this should be considered before other alterations are made.

tion may be desirable[34], excessive amounts should be avoided. This may require straightening vanes ahead of the impeller and rearranging the suction piping to avoid changes in direction or other obstructions. The cavitation damage to the impeller shown in Figure 20 was believed to have been at least partly due to bad flow conditions produced by two 90° elbows in the suction piping. The planes of the elbows were at 90° to each other, and this arrangement should be avoided.

Straightening vanes in the impeller inlet may increase the *NPSH* requirement at all flow rates. Three or four radial ribs equally spaced around the inlet and extending inward about one-quarter of the inlet diameter are effective against excessive prerotation and may require less *NPSH* than full-length vanes. This is very important with axial-flow pumps, which are apt to have unfavorable cavitation characteristics at partial flow rates. Operation near the best efficiency point usually minimizes cavitation.

The admission of a small amount of air into the pump suction tends to reduce cavitation noise.[7] This rarely is done, however, because it is difficult to inject the right amount of air under varying head and flow rate conditions and frequently there are objections to mixing air with the liquid pumped.

If a new impeller is required because of cavitation, the design should take into account the most recent advances described in the literature. Gongwer[35] has suggested (1) the use of ample fillets where the vanes join the shrouds, (2) sharpened leading edges of vanes, (3) reduction of β, in the immediate vicinity of the shrouds, and (4) raking the leading edges of the vanes forward out of the eye. Increasing the number of vanes for propeller pumps lowers σ for a given submergence. A change in the impeller material may be very beneficial, as described below.

Resistance of Materials to Cavitation Damage Table 8 shows the relative resistance of several metals to cavitation pitting produced by magnetostriction vibration. It will be seen that cast iron, the most commonly used material for impellers, has relatively little pitting resistance relative to bronze and stainless steel, which are readily cast and finished.

Damage due to cavitation erosion is commonly assessed in terms of the depth of penetration. The life of an impeller is generally considered to be the time required for cavitation erosion to reach a depth of 75% of the blade thickness at any point[36]. The life of any material in years can be expressed as the product of the mean depth of penetration rate

TABLE 8 Cavitation erosion resistance of metals

Alloy	Magnetostriction weight loss after 2 h, mg
Rolled stellite[a]	0.6
Welded aluminum bronze	3.2
Cast aluminum bronze	5.8
Welded stainless steel (2 layers, 17 Cr-7 Ni)	6.0
Hot rolled stainless steel (26 Cr-13 Ni)	8.0
Tempered rolled stainless steel (12 Cr)	9.0
Cast stainless steel (18 Cr-8 Ni)	13.0
Cast stainless steel (12 Cr)	20.0
Cast manganese bronze	80.0
Welded mild steel	97.0
Plate steel	98.0
Cast steel	105.0
Aluminum	124.0
Brass	156.0
Cast iron	224.0

[a]Despite the high resistance of this material to cavitation damage, it is not suitable for ordinary use because of its comparatively high cost and the difficulty encountered in machining and grinding.

Source: Reference 69.

(*MDPR*, in mm per year) times the thickness of the material in mm. Values of MDPR have been deduced[37] from the weight loss of test samples of known diameter in a magnetostriction test (Table 8)[38]. Unfortunately, *MDPR*-values obtained in such tests are not the same as those of actual pumps, as the mode of cavitation varies with pump operating conditions and is generally different from the laboratory results. Nevertheless, laboratory results for *MDPR* have been used to rank the ability of various materials to resist cavitation erosion in pumps. See Section 5.1 for material selection guidelines.

Cavitation-resistant coatings, either metallic or nonmetallic, have found some niche applications. Elastomeric coatings are resilient and resist cavitation through a different erosion mechanism than that of metal. As such, they can be very effective[69]. At least two considerations are involved in the use of coatings for resisting cavitation damage: 1) even if a contemplated coating demonstrates a reduced damage or erosion rate, this reduction must be enough to justify the cost of establishing a satisfactory bond between the coating and the base metal; 2) erosion of both the coating and the base material must be considered in determining the life according to the above 75%-depth criterion. Therefore, the life in this case would be equal to the *MDPR* of the coating times the coating thickness plus the *MDPR* of the base material times the allowable erosion depth of that material.

Inducers It is sometimes difficult or impossible to provide the required *NPSH* for an otherwise acceptable pump. Besides normal industrial situations that might produce a very low available *NPSH,* the need to keep the weight down in aircraft and rocket liquid-propellant pumps has led to high rotative speeds, which, for typical values of *NPSH,* produce extremely high suction specific speeds. The performance-*NPSH* required by the impeller under these circumstances can be provided by a small, axial-flow booster pump, called an inducer, placed ahead of the first-stage impeller[39]. Inducers are designed to operate with very low *NPSH* and to provide enough head to satisfy the *NPSH* required by the impeller. In fact, long stable cavities are established on the suction sides of the long, lightly-loaded blades of an inducer, which enable it to operate at about twice the suction specific speed of a conventional impeller[40,41]. At lower than normal flow rates, however, inducers readily produce swirling, destabilizing backflow at the inlet, which can cause excessive pump vibration in high-head pumps. These instabilities can be overcome by various passive design features, such as that described in Reference 39.

The inducers described in Reference 42 (Figure 30) have "constant lead" helical blades. They contribute not more than 5% of the total pump head. Although the efficiency of the inducer alone is low, the reduction in overall pump efficiency is not significant. Because this type of inducer causes prerotation, a careful match between inducer and suction impeller is required. In vertical multistage pumps, where a long shaft can be better supported, a vaned diffuser may be inserted between the inducer and the first-stage impeller. Such an arrangement is very beneficial for operation at reduced flow rate. Reference 42 shows that a suitable inducer-impeller combination can operate at about 50% of the *NPSH* required for the impeller alone at flow rates not exceeding the normal value. The *NPSH* requirement increases rapidly for flow rates above normal. Unless a variable-lead inducer is used[32, 39], operation in this range should be avoided.

Entrained Air Air or other gases may enter the impeller inlet from several sources. The immediate effect usually will be a drop in pump pressure rise, flow rate, and power. This will be followed by loss of prime if more gas is present than the impeller can handle. A typical limit for commercial industrial pumps is an inlet gas-to-liquid volume fraction (GVF) of 0.03, although specialty pumps such as those used in aircraft (Section 9.19) can handle higher GVF. See also Reference 9, Section 2.1. Air may be released from solution or enter through leaks in the suction piping. Stuffing box air leakage may be prevented by lantern rings supplied with liquid from the pump discharge. If the pump takes water from a sump with a free surface, a vortex may form from the free surface to the impeller inlet. The remedy may be the introduction of one or more baffle plates or even major changes in the sump. For information on proper sump design and the prevention of air-entraining vortices, see Sections 10.1 and 10.2, pp. 457 and 460 of Reference 7, and Reference 43. It is sometimes permissible to inject a small amount of air into the pump

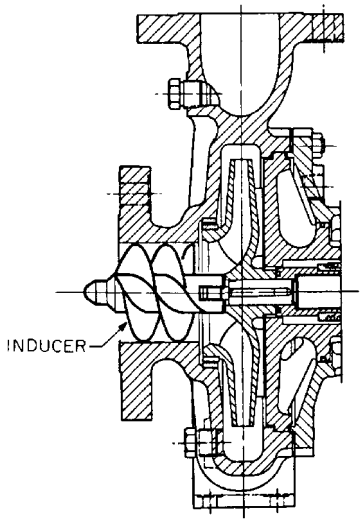

FIGURE 30 Pump fitted with inducer (Reference 42)

suction to reduce the noise and damage from cavitation caused by inadequate *NPSH* or recirculation in the impeller (see Subsection 2.3.2).

STARTING CENTRIFUGAL PUMPS

Priming Centrifugal pumps usually are completely filled with the liquid to be pumped *before starting*. When so filled with liquid, the pump is said to be *primed.* Pumps have been developed to start with air in the casing and then be primed.[44] This procedure is unusual with low-specific-speed pumps but is sometimes done with propeller pumps[12]. In many installations, the pump is at a lower elevation than the supply and remains primed at all times. This is customary for pumps of high specific speed and all pumps requiring a positive suction head to avoid cavitation.

Pumps operated with a suction lift may be primed in any of several ways. A relatively inexpensive method is to install a special type of check valve, called a foot *valve,* on the inlet end of the suction pipe and prime the pump by filling the system with liquid from any available source. Foot valves cause undesirable frictional loss and may leak enough to require priming before each starting of the pump. A better method is to close a valve in the discharge line and prime by evacuating air from the highest point of the pump casing. Many types of vacuum pumps are available for this service. A priming chamber is a tank that holds enough liquid to keep the pump submerged until pumping action can be initiated. Self-priming pumps usually incorporate some form of priming chamber in the pump casing. Section 2.4 and Reference 7 may be consulted for further details.

Torque Characteristics of Drivers Centrifugal pumps of all specific speeds usually have such low starting torques (turning moments) that an analysis of the starting phase of operation seldom is required. Steam and gas turbines have high starting torques, so no special starting procedures are necessary when they are used to drive pumps. If a pump is directly connected to an internal combustion engine, the starting motor of the engine should be made adequate to start both driver and pump. If the starter does not have enough torque to handle both units, a clutch must be provided to uncouple the pump until the driver is started.

Electric motors are the most commonly used drivers for centrifugal pumps. Direct current motors and alternating current induction motors usually have ample starting torque for all pump installations, provided the power supply is adequate. Many types of reduced voltage starters are available[7] to limit the inrush current to safe values for a given power supply. Synchronous motors are often used with large pumps because of their favorable power-factor properties. They are started as induction motors and run as such up to about 95% of synchronous speed. At this point, dc field excitation is applied and the maximum torque the motor can then develop is called the poll-in *torque,* which must be enough to accelerate the motor and connected inertia load to synchronous speed in about 0.2 s if synchronous operation is to be achieved. Centrifugal pumps usually require maximum torque at the normal operating point, and this should be considered in selecting a driver, particularly a synchronous motor, to be sure that the available pull-in torque will bring the unit to synchronous speed.

Torque Requirements of Pumps The *torque,* or turning moment, for a pump may be estimated from the power curve in USCS units by

$$M = \frac{5252P}{n} \tag{25}$$

and in SI units by

$$M = \frac{9549P}{n}$$

where M = pump torque, lb · ft (N · m)
P = power, hp (kW)
n = speed, rpm

Equation 25 makes no allowance for accelerating the rotating elements or the liquid in the pump. If a 10% allowance for accelerating torque is included, the constant should be correspondingly increased. The time Δt required to change the pump speed by an amount $\Delta n = n_2 - n_1$ is given by

$$\Delta t = \frac{I\Delta n}{k(M_m - M)} \tag{26}$$

where Δt = time, s
I = moment of inertia (flywheel effect) of all rotating elements of driver, pump, and liquid, lb · ft (kg · m^2)
Δn = change in speed, rpm
k = 307 in USCS (9.549 in SI)
M_m = driver torque, lb · ft (N · m)
M = pump torque, lb · ft (N · m) (Eq. 25)

The inertia I of the driver and pump usually can be obtained from the manufacturers of the equipment. The largest permissible Δn for accurate calculation will depend on how rapidly M_m and M vary with speed. The quantity $M_m - M$ should be nearly constant over the interval Δn if an accurate estimate of Δt is to be obtained. Torque-speed characteristics of electric motors may be obtained from the manufacturers.

Horizontal-shaft pumps fitted with plain bearings and packed glands require a *breakaway torque* of about 15% of M_n, the torque at the normal operating point, to overcome the static friction. This may be reduced to about 10% of M_n if the pump is fitted with antifriction bearings. The breakaway torque may be assumed to decrease linearly with speed to nearly zero when the speed reaches 15 to 20% of normal. Construction of torque-speed curves requires a knowledge of the pump characteristics at normal speed as well as details of the entire pumping system. Some typical examples taken from Reference 7 are given

below. The following forms of the affinity laws (Eqs. 12) are useful in constructing the various performance curves:

$$Q_2 = Q_1 \frac{n_2}{n_1} \tag{27}$$

$$H_2 = H_1\left(\frac{n_2}{n_1}\right)^2 = H_1\left(\frac{Q_2}{Q_1}\right)^2 \tag{28}$$

$$P_2 = P_1\left(\frac{n_2}{n_1}\right)^3 \tag{29}$$

$$M_2 = M_1\left(\frac{n_2}{n_1}\right)^2 \tag{30}$$

where Q = flow rate
n = speed
H = head
P = power
M = torque

in any consistent units of measure. After speeds n_1 and n_2 are chosen, the subscripts 1 and 2 refer to corresponding points on the characteristic curves for these speeds.

Low-Specific-Speed Pumps Figure 31 shows the constant-speed characteristics of a pump having $n_s \approx 1740$ (0.64) at best efficiency. This pump usually would be started with a valve in the discharge line closed. During the starting phase, the pump operates at shutoff with $P_1 = 25.8$ hp (19.2 kW) and $n_1 = 1770$ rpm. Then, by Eq. 25, $M_1 = 76.6$ lb · ft (103.9 $N \cdot m$). These values may be used in Eq. 30 to evaluate starting torques M_2 at as many speeds n_2 as desired and plotted in Figure 32 as curve *BCD*. Section *AB* of the starting torque curve is an estimate of the breakaway torque. If the discharge valve is now opened, the speed remains nearly constant but the torque increases as the capacity and power increase. If the normal operating point is $Q = 1400$ gpm (88.3 l/s) and $P_n = 53.2$ hp (39.7 kW), the motor torque will be $M_n = 158$ lb · ft (214 $N \cdot m$) by Eq. 25. The vertical line DE in Figure 32 shows the change in torque produced by opening the discharge valve.

Instead of starting the pump with the discharge valve closed, let the pump be started with a check valve in the discharge line held closed by a static head of 100 ft (30.5 m). The frictional head in the system may be represented by kQ^2. The value of k may be estimated from the geometry of the system or from a frictional-loss measurement at any convenient flowrate Q, preferably near the normal capacity Q_n. In this example, $Q_n = 1400$ gpm (88.33 l/s) and $k = 14.4/10^6$ (0.00109). The curve labeled system head 1 in Figure 31 was computed from $H = 100 + (14.4/10^6)Q^2$ ft ($H = 30.48 + 0.00109Q^2$ m) and intersects the head curve at $H = 128$ ft (39.01 m) and $Q_n = 1400$ gpm (88.33 l/s). The normal shutoff head is $H_1 = 153$ ft (46.6 m) at $n_1 = 1770$ rpm. By Eq. 28, the pump will develop a shutoff head $H_2 = 100$ ft (30.5 m) at $n_2 = 1430$ rpm. By Eq. 30, the torque at 1430 rpm will be 50 lb · ft (68 $N \cdot m$), corresponding to point *C* in Figure 32. The portion ABC of the starting torque curve has already been constructed. Trial-and-error methods must be used to obtain the portion *ABC* of the starting torque curve.

The auxiliary curves in Figure 33 are useful in constructing the *CE* portion of the starting torque curve. Select a value of n_2 intermediate between 1427 and 1770 rpm, say $n_2 = 1600$ rpm. In Figure 31, read values of Q_1, H_1, and P_1 for speed $n_1 = 1770$ rpm. By Eqs. 27 and 28, determine values of Q_2 and H_2 and plot as shown in Figure 31 until an intersection with the system-head 1 curve is obtained that provides Q_{1600} corresponding to $n = 1600$ rpm. By Eq. 29, determine value of P_2 and plot as shown in Figure 31 until an intersection is obtained with the Q_{1600} line which provides P_{1600} corresponding to $n = 1600$ rpm. Eq. 34 is now used to obtain M_{1600}, which is one point on the desired starting torque curve. The process is repeated for various speeds n_2 until the curve *CE* in Figure 32 can be drawn. The

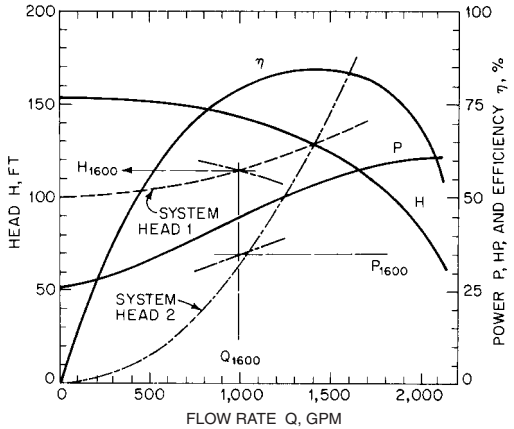

FIGURE 31 Characteristics of a 6-by-8 double-section pump at 1770 rpm (ft × 0.3048 = m; gpm × 0.06309 = l/s; hp × 0.7457 = kW) $n_s = 1{,}740$ ($\Omega_s = 0.64$) (Reference 7)

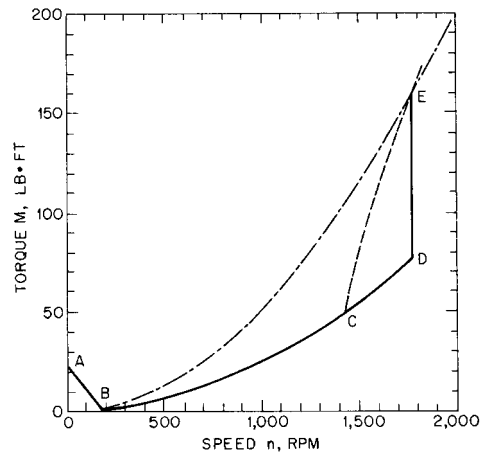

FIGURE 32 Torque characteristics of 6-by-8 pump shown in Figure 31 (lb • ft × 1.356 = N • m) (Reference 7)

complete starting torque curve for this example is *ABCE* in Figure 31, with steady-state operation at point *E*.

Assume that the pump of the preceding examples is installed in a system having zero static head but a long pipeline with friction head given by $H = (65.4/10^6)Q^2$ ft ($H = 0.00500Q^2$ m), as shown in Figure 31 by the curve labeled system head 2. The valve in the discharge line is assumed to open instantaneously when power is first applied to the pump. The procedure described to construct curve *CE* of the preceding example must now be used together with the system-head 2 curve of Figure 31 to obtain the curve *BE* of Figure 32. The complete starting torque curve for this example is *ABE* in Figure 32, with steady-state operation at point *E*.

The inertia of the fluid in the system was neglected in solving the previous examples. Some of the power must be used to accelerate the liquid, and this may be appreciable in the case of a long pipeline. Low-specific speed pumps, which are used with long pipelines, have

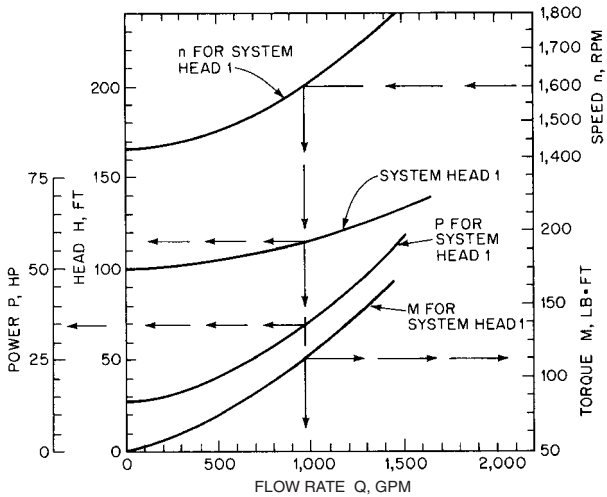

FIGURE 33 Analysis of 6-by-8 pump shown in Figure 41 (ft × 0.3048 = m; gpm × 0.06309 = l/s; lb • ft × 1.356 = N • m; hp × 0.7457 = kW) (Reference 7)

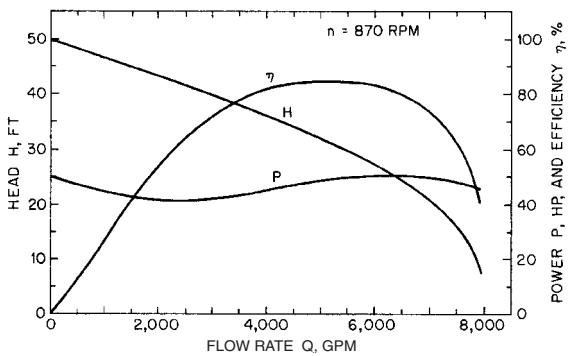

FIGURE 34 Characteristics of a 16-in (40.6cm) volute pump with mixed-flow impeller with flat power characteristic (ft × 0.3048 = m; gpm × 0.06309 = l/s; hp × 0.7457 = kW). n_s = 4570 (Ω_s = 1.672) (Reference 7)

rising power curves with minimum power at shutoff and maximum power at normal flow rate. Experience has shown that the starting torque-speed curves computed by neglecting the inertia of the liquid are conservative, so inertia effects need not be included. The inertia effect of the liquid does slow the starting operation. If the time required to reach any event, such as a particular speed or flow rate, is required, the inertia of the liquid should be considered, but including it greatly increases the difficulty of computation. References 45 through 48 give general methods for handling problems involving liquid transients.

High-specific-speed pumps have falling power flow rate curves with maximum power at shutoff and minimum power at normal flow rate. Neglecting the inertia of the liquid probably will result in too low a value for the computed starting torque for such pumps. If liquid inertia is to be included, consult References 44 to 47 and Section 8.1.

MEDIUM- AND HIGH-SPECIFIC-SPEED PUMPS Figure 34 shows constant-speed characteristics for a medium-specific-speed pump, n_s = 4570 (1.672) at best efficiency. The shutoff power

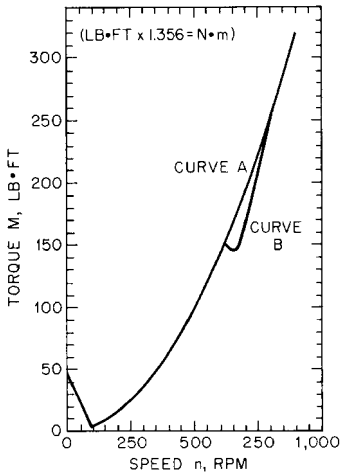

FIGURE 35 Torque characteristics of pump shown in Figure 34 (Reference 7)

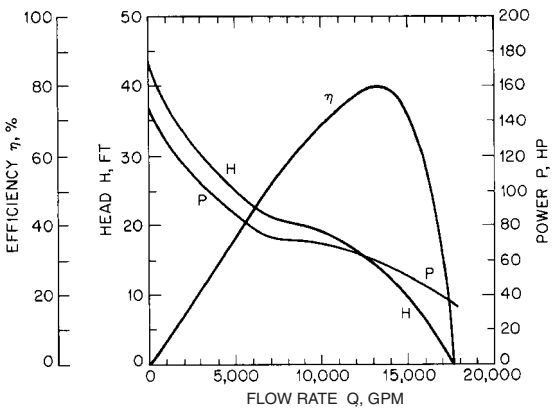

FIGURE 36 Characteristics of a 30-in (76.2-cm) discharge propeller pump at 700 rpm (ft × 0.1048 = m; gpm × 0.06309 = l/s; hp × 0.7457= kW). n_s = 12,000 (Ω_s = 4.391) (Reference 7)

is the same as the power at best efficiency, and the starting torque-speed curve is but little affected by the method of starting, as shown by Figure 35.

Figure 36 shows the constant-speed characteristics of a high-specific-speed propeller pump, $n_s \approx$ 12,000 (4.391) at best efficiency. Figure 37 shows the starting torque-speed curve when the pump is started against a static head of 14 ft (4.3 m) and a friction head of 1 ft (0.3 m) at Q_n = 12,500 gpm (789 l/s). The system was assumed full of water with a closed check valve at the outlet end of the short discharge pipe. The methods of computation for Figures 35 and 37 were the same as for Figure 32.

Sometimes propeller pumps are started with the pump submerged but with the discharge column filled with air. In such a case, the torque-time characteristic for the driver must be known and a step-by-step calculation carried out. If the discharge column is a siphon initially filled with air, the starting torque may exceed the normal running torque during some short period of the starting operation. If the pump is driven by a synchronous

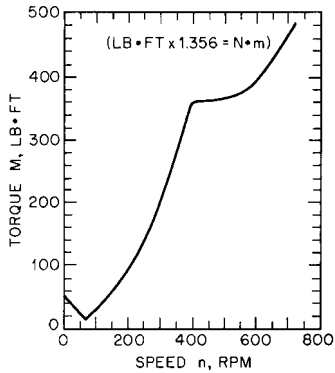

FIGURE 37 Torque characteristics of pump shown in Figure 36 (Reference 7)

motor, it is particularly important to investigate the starting torque in the range of 90 to 100% of normal speed to make sure that the pull-in torque of the motor is not exceeded. For additional information regarding starting high-specific-speed pumps discharging through long and large diameter systems, see Section 8.1.

Miscellaneous Requirements Pumps handling hot liquids should be warmed up to operating temperature before being started unless they have been especially designed for quick starting. Failure to do this may cause serious damage to wearing rings, seals, and any hydraulic balancing device that may be present. A careful check of the installation should be made before starting new pumps, pumps that have had a major overhaul, or pumps that have been standing idle for a long time. It is very important to follow the manufacturer's instructions when starting boiler-feed pumps. If these are unavailable, Reference 7 may be consulted. Ascertain that the shaft is not frozen, that the direction of rotation is correct, preferably with the coupling disengaged, and that bearing lubrication and gland cooling water meet normal requirements. Failure to do this may result in damage to the pump or driver.

A pump may run backwards at runaway speed if the discharge valve fails to close following shutdown. Any attempt to start the pump from this condition will put a prolonged overload on the motor. Figure 38 shows one example of the torque-speed transient for a pump, $n_s = 1700\ (0.622)$, started from a runaway reversed speed while normal pump head was maintained between the section and discharge flanges. In most practical cases, water hammer effects would make this transient even more unfavorable than Figure 38 indicates. The duration of such a transient will always be much longer than the normal starting time, and so protective devices would probably disconnect the motor from the power supply before normal operation could be achieved. Consult Section 8.1 for additional information on this subject.

REGULATION OF FLOW RATE

Flow rate variation ordinarily is accomplished by a change in pump head, speed, or both simultaneously. The flow rate and power input of pumps with specific speeds up to about 4000 (1.464) double suction increase with decreasing head, so the drivers of such pumps may be overloaded if the head falls below a safe minimum value. Increasing the head of high-specific-speed pumps decreases the flow rate but increases the power input. The drivers of these pumps should either be able to meet possible load increases or be equipped with suitable overload protection. Flow rate regulation by the various methods given below may be manual or automatic (see also References 1, 7, 12, 34 and 49).

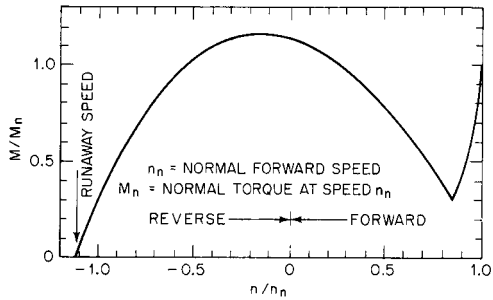

FIGURE 38 Torque characteristics of a double-suction pump, $n_s \approx 1700$ (0.64), from reversed runaway speed to normal forward speed (Reference 7)

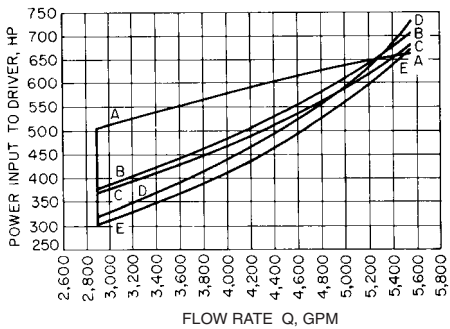

FIGURE 39 Power requirements of two double-suction pumps in series operated at constant head and variable flow rate. Total H_n = 382 ft (116 m) for both pumps at 1800 rpm (gpm × 0.06309 = l/s hp × 0.7457 = kW) (Reference 50). Curve *AA:* constant speed with discharge throttling. Curve *BB:* synchronous motor with variable-speed hydraulic coupling on each pump. Curve *CC*: variable-speed wound-rotor induction motor. Curve *DD:* dc motor with rectifier and shunt field control. Curve *EE:* synchronous motor with variable-speed constant-efficiency mechanical speed reducer

Discharge Throttling This is the cheapest and most common method of flow rate modulation for low- and medium- specific-speed pumps. Usually its use is restricted to such pumps. Partial closure of any type of valve in the discharge line will increase the system head so the system-head curve will intersect the pump head curve at a smaller flow rate, as shown in Figure 40. Discharge throttling moves the operating point to one of lower efficiency, and power is lost at the throttle valve. This may be important in large installations, where more costly methods of modulation may be economically attractive. Throttling to the point of cutoff may cause excessive heating of the liquid in the pump. This may require a bypass to maintain the necessary minimum flow or use of different method of modulation. This is particularly important with pumps handling hot water or volatile liquids, as previously mentioned. Refer to Section 8.2 for information regarding the sizing of a pump bypass.

Suction Throttling If sufficient *NPSH* is available, some power can be saved by throttling in the suction line. Jet engine fuel pumps frequently are suction throttled[5] because discharge throttling may cause overheating and vaporization of the liquid. At very low flow rate, the impellers of these pumps are only partly filled with liquid, so the power input and temperature rise are about one-third the values for impellers running full with discharge throttling. The capacity of condensate pumps frequently is submergence-controlled,[7] which

is equivalent to suction throttling. Special design reduces cavitation damage of these pumps to a negligible amount, the energy level (Section 2.1) being quite low.

Bypass Regulation All or part of the pump flow may be diverted from the discharge line to the pump suction or other suitable point through a bypass line. The bypass may contain one or more metering orifices and suitable control valves. Metered bypasses are commonly used with boiler-feed pumps for reduced-flow operation, mainly to prevent overheating. There is a considerable power saving if excess capacity of propeller pumps is bypassed instead of using discharge throttling.

Speed Regulation This can be used to minimize power requirements and eliminate overheating during flow rate modulation. Steam turbines and internal combustion engines are readily adaptable to speed regulation at small extra cost. A wide variety of variable-speed mechanical, magnetic, and hydraulic drives are available, as well as both ac and dc variable-speed motors. Usually variable-speed motors are so expensive that they can be justified only by an economic study of a particular case. Figure 39 shows a study by Richardson[50] of power requirements with various drivers wherein substantial economies in power may be obtained from variable-speed drives.

Regulation by Adjustable Vanes Adjustable guide vanes ahead of the impeller have been investigated and found effective with a pump of specific speed $n_s = 5700$ (2.086). The vanes produced a positive prewhirl that reduced the head, flow rate, and efficiency. Relatively little regulation was obtained from the vanes with pumps having $n_s = 3920$ (1.204) and 1060 (0.39). Adjustable outlet diffusion vanes have been used with good success on several large European storage pumps for hydroelectric developments. Propeller pumps with adjustable-pitch blades have been investigated with good success. Wide flow rate variation was obtained at constant head and with relatively little loss in efficiency. These methods are so complicated and expensive that they have very limited application in practice. Reference 34 may be consulted for further discussion and bibliography.

Air Admission Admitting air into the pump suction has been demonstrated as a means of flow-rate regulation, with some savings in power over discharge throttling. Usually air in the pumped liquid is undesirable, and there is always the danger that too much air will cause the pump to lose its prime. The method has rarely been used in practice but might be applicable to isolated cases.

PARALLEL AND SERIES OPERATION

Two or more pumps may be arranged for parallel or series operation to meet a wide range of requirements in the most economical manner. If the pumps are close together, that is, in the same station, the analysis given below should be adequate to secure satisfactory operation. If the pumps are widely separated, as in the case of two or more pumps at widely spaced intervals along a pipeline, serious pressure transients may be generated by improper starting or stopping procedures. The analysis of such cases may be quite complicated, and References 46 to 48 should be consulted for methods of solution.

Parallel Operation Parallel operation of two or more pumps is a common method of meeting variable-flow-rate requirements. By starting only those pumps needed to meet the demand, operation near maximum efficiency can usually be obtained. The head-flow characteristics of the pumps need not be identical, but pumps with unstable characteristics may give trouble unless operation only on the steep portion of the characteristic can be assured. Care should be taken to see that no one pump, when combined with pumps of different characteristics, is forced to operate at flows less than the minimum required to prevent recirculation. See the discussion that follows on operation at other than normal flow rate. Multiple pumps in a station provide spares for emergency service and for the downtime needed for maintenance and repair.

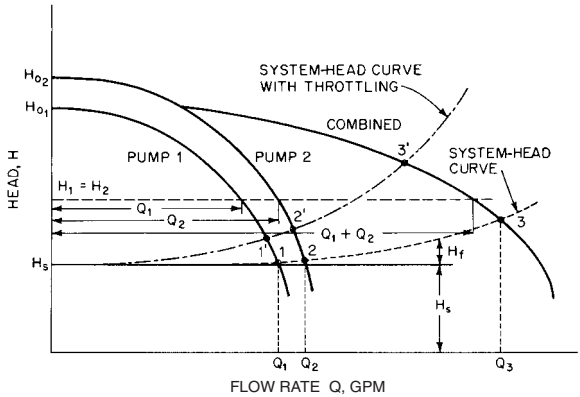

FIGURE 40 Head-flow curves of pumps operating in parallel

The possibility of driving two pumps from a single motor should always be considered, as it usually is possible to drive the smaller pumps at about 40% higher speed than a single pump of twice the capacity. The saving in cost of the higher-speed motor may largely offset the increased cost of two pumps and give additional flexibility of operation.

One of the first steps in planning for multiple-pump operation is to draw the system-head curve, as shown in Figure 40. The system head consists of the static head H_s and the sum H_f of the pipe-friction head and the head lost in the valves and fittings (see Sections 8.1 and 8.2). The head curves of the various pumps are plotted on the same diagram, and their intersections with the system-head curve show possible operating points. *Combined pump head curves* are drawn by adding the flow rates of the various combinations of pumps for as many values of the head as necessary. The intersection of any combined *H-Q* curve with the system-head curve is an operating point. Figure 40 shows two pump head curves and the combined curve. Points 1, 2, and 3 are possible operating conditions. Additional operating points may be obtained by changing the speed of the pumps or by increasing the system-head loss by throttling. Any number of pumps in parallel may be included on a single diagram, although separate diagrams for different combinations of pumps may be preferable.

The overall efficiency η of pumps in parallel is given by

$$\eta = \frac{H(\text{sp. gr.})}{k} \times \frac{\Sigma Q}{\Sigma P} \tag{31}$$

where H = head, ft (m)
sp. gr. = specific gravity of the liquid
k = 3960 USCS (0.1021 SI)
ΣQ = sum of the pump flow rates, gpm (l/s)
ΣP = total power supplied to all pumps, hp (W)

Series Operation Pumps are frequently operated in series to supply heads greater than those of the individual pumps. The planning procedure is similar to the case of pumps in parallel. The system-head curve and the individual head-flow curves for the pumps are plotted as shown in Figure 41. The pump heads are added as shown to obtain the combined pump head curve. In this example, Pump 2 operating alone will deliver no liquid because its shutoff head is less than the system static head.

There are two possible operating points, 1 and 2, as shown by the appropriate intersections with the system-head curve. As with parallel operation, other operating points

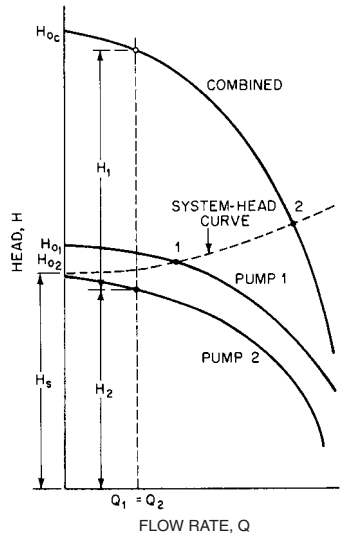

FIGURE 41 Head-flow curves of pumps operating in series

could be obtained by throttling or by changing the pump speeds. The overall efficiency of pumps in series is given by

$$\eta = \frac{Q(\text{sp. gr.})}{k} \times \frac{\Sigma H}{\Sigma P} \tag{32}$$

wherein the symbols are the same as for parallel operation. It is important to note that the stuffing box pressure of the second pump is increased by the discharge pressure of the first pump. This may require a special packing box for the second pump with leakoff to the suction of the first pump. The higher suction pressure may increase both the first cost and the maintenance costs of the second pump.

OPERATION AT OTHER THAN THE NORMAL FLOW RATE

Centrifugal pumps usually are designed to operate near the point of best efficiency, but many applications require operation over a wide range of flow rates, including shutoff, for extended periods of time. Pumps for such service are available but may require special design and construction at higher cost. Noise, vibration, and cavitation may be encountered at low flow rates. Large radial shaft forces at shutoff as well as lack of through flow to provide cooling may cause damage or breakage to such parts as shafts, bearings, seals, glands, and wearing rings of pumps not intended for such service. Some of the phenomena associated with operation at other than normal flow rate are described below.

Recirculation There is a small flow from impeller discharge to suction through the wearing rings and any hydraulic balancing device present. This takes place at all flow rates, but does not usually contribute to raising the liquid temperature very much unless operation is near shutoff.

When the flow rate has been reduced by throttling (or as a result of an increase in system head), a secondary flow called *recirculation* begins. Recirculation is a flow reversal due to separation at the suction and at the discharge tips of the impeller vanes. All impellers

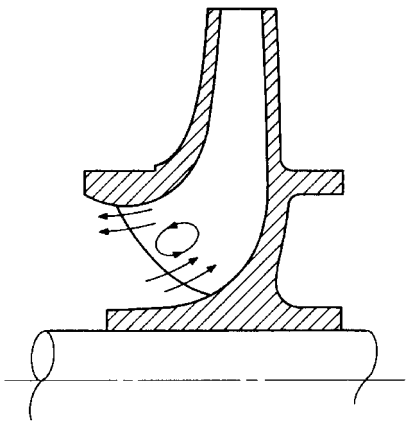

FIGURE 42 Suction recirculation

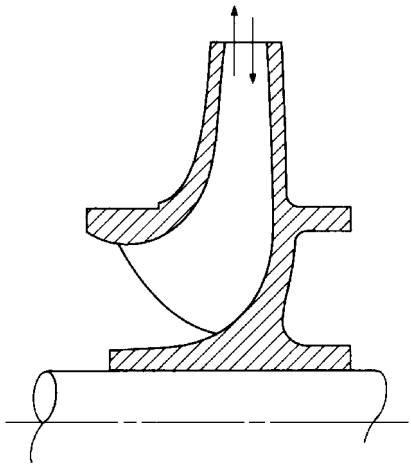

FIGURE 43 Discharge recirculation

have a critical flow rate at which recirculation occurs. The flow rates at which suction and discharge recirculation begin can be controlled to some extent by design, but recirculation cannot be eliminated (see Figure 6 in Section 2.1).

Suction recirculation is the reversal of flow at the impeller eye. A portion of the flow is directed out of the eye at the eye diameter, as shown in Figure 42 , and travels upstream with a rotational velocity approaching the peripheral velocity of the diameter. A rotating annulus of liquid is produced upstream from the impeller inlet, and through the core of this annulus passes an axial flow corresponding to the output flow rate of the pump. In pumps equipped with long, straight suction nozzles but no suction elbow, this rotating fluid has been detected over considerable distances upstream from the impeller eye. Suction pressures measured at wall taps where this phenomenon is present are always higher than the true average static pressure across the measuring section. This means that the pump head as determined from wall taps is less than it would be if true average static pressures were measured. The high shear rate between the rotating annulus and the axial flow through the core produces vortices that form and collapse, producing noise and cavitation in the suction of the pump.

Discharge recirculation is the reversal of flow at the discharge tips of the impeller blades, as shown in Figure 43. The high shear rate between the inward and outward relative velocities produces vortices that cavitate and can attack the pressure side of the blades. This phenomenon, which tends to occur at a lower flow rate than the highest Q for suction recirculation, also involves stalled flow from the diffuser vanes or volute tongue(s). Separated reversed flow recirculates and emerges from these vane systems back into the impeller with negative swirl (that is, swirl opposite to the direction of rotation). The impeller must expend significant power to redirect the portion of this fluid (that reenters it) out again—with positive swirl. As discussed in Section 2.1, the portion of this backflow from the diffuser or volute that enters the spaces outside the impeller shrouds and adjacent to the casing walls has the potential to reverse the axial thrust of the impeller, and this reversal can fluctuate if the backflow is unsteady (as separated, recirculating flow normally is) and not always feeding the same side of the impeller.

The flow rate Q_{sr} below which suction recirculation occurs is directly related to the design suction-specific speed S of the pump. The higher the suction-specific speed, the closer will be the beginning of recirculation to the flow rate at best efficiency. Figure 44 shows the relation between the suction specific speed and suction recirculation for pumps

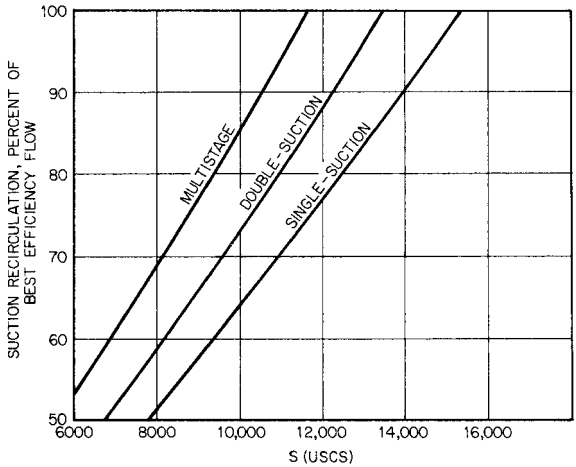

FIGURE 44 Influence of the design value of suction specific speed S on the flow rate Q_{SR} below which suction recirculation occurs. $500 < n_s < 2500$; $(0.18 < \Omega_s < 0.91)$ for single-suction or one side of a double-suction impeller. The ordinate is Q_{SR}/Q_{BEP} in percent. (To obtain Ω_{ss}, divide S by 2733.)

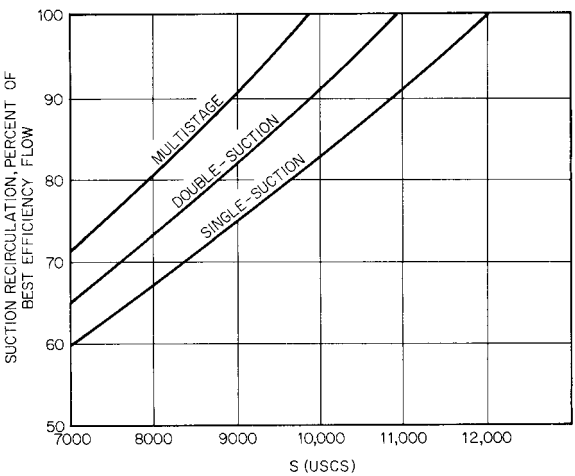

FIGURE 45 Influence of the design value of suction specific speed S on the flow rate Q_{SR} below which suction recirculation occurs. $2500 < n_s < 10{,}000$; $(0.91 < \Omega_s < 3.66)$ for single-suction or one side of a double-suction impeller. The ordinate is Q_{SR}/Q_{BEP} in percent. (To obtain Ω_{ss}, divide S by 2733.)

up to 2500 (0.915) specific speed, and Figure 45 shows the same relation for pumps up to 10,000 (3.659) specific speed.

Despite the existence of suction and discharge recirculation, the mechanical response of the pump will not be serious unless the energy level is high. In other words, most pumps can indeed be operated at $Q < Q_{SR}$. The minimum flow rate or simply "minimum flow" $Q_{\min}$ is quantified in Section 2.1. As energy level is increased, $Q_{\min}$ approaches Q_{SR} in the limit. Examples of the difference between $Q_{\min}$ and Q_{SR} are as follows: For water pumps rated at 2500 gpm (158 l/s) and 150 ft (45.7 m) total head or less, the minimum operating flows can

be as low as 50% of the suction recirculation values shown for continuous operation and as low as 25% for intermittent operation. For hydrocarbons, the minimum operating flows can be as low as 60% of the suction recirculation values shown for continuous operation and as low as 25% for intermittent operation.[51, 52, 53]

Temperature Rise Under steady-state conditions, friction and the work of compression increase the temperature of the liquid as it flows from suction to discharge. A further temperature increase may arise from liquid returned to the pump suction through wearing rings, a balancing device, or a minimum-flow bypass line that protects the pump when operating at or near shutoff.

Assuming that all heat generated remains in the liquid, the temperature rise is

$$\Delta T = \frac{gH \times (1 - \eta)}{g_o C_p \eta J} + \Delta T_c \tag{33}$$

where $g/g_o = 1$ lbf/lbm; but when using SI units, g/g_o is replaced by 9.80665 m/s^2 (= g in the SI system). ΔT_c is due to the compression of the liquid and is not a consequence of loss or dissipation as is the term involving the pump efficiency η (see Section 2.1). As shown in Reference 1 of Section 2.1, ΔT_c is 3°F per 1000 psi (0.24°C per MPa) of pump pressure rise for hydrocarbon fuels. For boiler feedwater at 350°F (177°C), ΔT_c = 1.6°F per 1000 psi (0.129°C per MPa), but it is much smaller for cold water. By consulting tables of properties for the liquid phase of the fluid being pumped and assuming the compression process between the actual inlet and discharge pressures to be isentropic, ΔT_c can be determined. This is important if Eq. 33 is used to evaluate overall pump efficiency from temperature rise measurements. ΔT and ΔT_c are often of the same order of magnitude at BEP, and serious errors have been made by excluding ΔT_c from the efficiency computation. At very low, off-BEP flow rates, ΔT will be high in comparison to ΔT_c; so, the latter can be safely ignored in temperature rise calculations at such low-efficiency conditions.

In practice, determination of efficiency from ΔT-measurements is accomplished by the direct thermodynamic method[54], rather than by the ΔT_c-method. Both approaches are based on the definition of pump efficiency as the ratio of an isentropic rise of total enthalpy (= $g\Delta$H) to the actual rise of total enthalpy (Eq. 1 of Section 2.1), allowances being made for the usually small external power losses that do not appear in the pumped fluid (such as bearing drag) and the similarly small effects of heat transferred between pump and surroundings. In the direct thermodynamic method, the enthalpy rise Δh is found from the chain rule,

$$\Delta h = \int dh = \int [(\partial h/\partial p)_T dp + (\partial h/\partial T)_p dT] = a\Delta p + C_p J \Delta T$$

the coefficients a and $C_p J$ being average values of the two partial derivatives as found from tables of thermodynamic properties of the fluid. Values of these partial derivatives are conveniently tabulated for water in Reference 54.

General service pumps handling cold liquids may be able to stand a temperature rise as great as 100°F (56°C). Most modern boiler-feed pumps may safely withstand a temperature rise of 50°F (28°C). The NPSH required to avoid cavitation or to prevent flashing of hot liquid returned to the pump suction may be the controlling factor. Minimum flow may be dictated by other factors, such as recirculation and unbalanced radial and axial forces on the impeller. Axial forces can be the controlling factor with single-stage double-suction pumps.

It is especially important to protect even small pumps handling hot liquids from operation at shutoff. This is usually done by providing a bypass line fitted with a metering orifice to maintain the minimum required flow through the pump. In the case of boiler-feed pumps, the bypass flow usually is returned to one of the feed-water the water heaters. Unless especially designed for cold starting, pumps handling hot liquids should be warmed up gradually before being put into operation.

Radial Thrust Ideally, the circumferential pressure distribution at the impeller exit is uniform at the design condition (as explained in Section 2.1); however, it becomes non-

uniform at off-BEP flow rates. An exception is that concentric collecting configurations will produce non-uniform pressure distributions at the BEP. Any non-uniformity leads to a radial force on the pump shaft called the radial thrust or radial reaction. The radial thrust F_r in pounds (newtons) is

$$F_r = kK_r(\text{sp. gr.})HD_2b_2 \tag{34}$$

where k = 0.433 USGS (9790 SI)
K_r = experimentally determined coefficient
sp. gr. = specific gravity of the liquid pumped (equal to unity for cold water)
H = pump head, ft (m)
D_2 = outside diameter of impeller, in (m)
b_2 = breadth of impeller at discharge, including shrouds, in (m)

Values of K_r determined by Agostinelli et al.[55] for single-volute pumps are given in Figure 46 as functions of specific speed and flow rate. The magnitude and direction of F_r on the pump shaft may be estimated from Figure 47 , but Eq. 34 probably will be more accurate for determining the magnitude of the force. The radial thrust usually is minimum near $Q = Q_n$, the flow rate at best efficiency, but rarely goes completely to zero. Near shutoff, F_r usually is maximum and may be a considerable force on the shaft in high-head pumps.

The radial thrust can be made much smaller throughout the entire flow-rate range by using a double volute (twin volute) or a concentric casing. These designs should be considered, particularly if the pump must operate at small flow rates. Figures 48 to 50 compare radial forces generated by three types of casings: a standard volute, a double volute, and a modified concentric casing. The latter casing was concentric with the impeller for 270° from the tongue and then enlarged in the manner of a single volute to form the discharge nozzle. The magnitude and direction of F_r on the pump shaft for the modified concentric casing may be estimated from Figure 51. The direction of F_r on the pump shaft with a double volute was somewhat random but in the general vicinity of the casing tongue. Radial forces on pumps fitted with diffuser vanes usually are rather small, although they may be significant near shutoff due to stall in some of the passages and not in others.

EXAMPLE Consider a single-stage centrifugal pump, n_s = 2000 (0.732) at best efficiency, handling cold water, sp. gr. = 1.0. Estimate the radial thrust on the impeller at half the normal flow rate when fitted with (a) a single volute, (b) a modified concentric casing, and (c) a double volute. Impeller dimensions are D_2 = 15.125 in (38.4 cm) and b_2 = 2.5 in (6.35 cm). The shutoff head is H = 252 ft (76.8 m), and the head at half capacity is H = 244 ft (74.4 m).

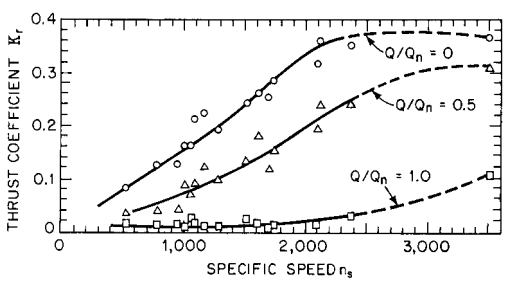

FIGURE 46 K_r as a function of specific speed and flow rate for single-volute pumps (to obtain Ω_s, divide by 2733.) (Reference 55)

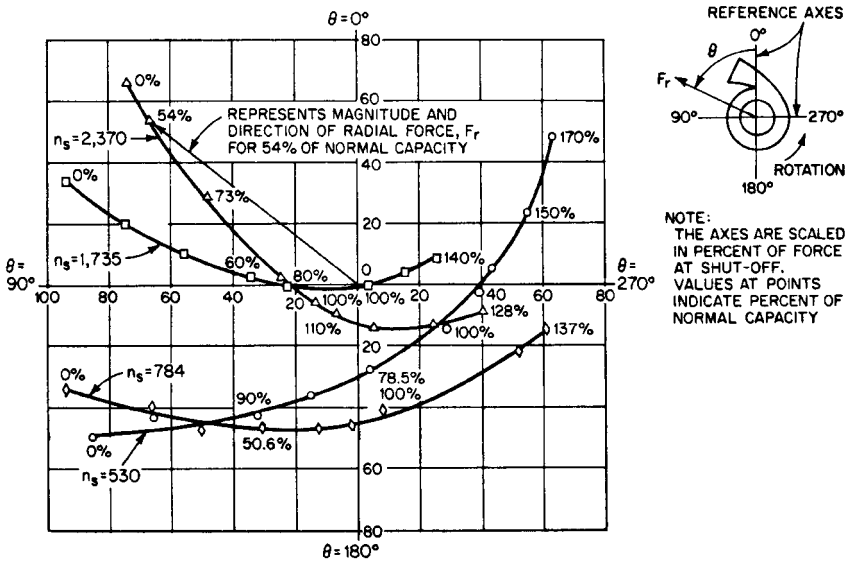

FIGURE 47 Polar plot showing direction of resultant radial forces for single-volute pumps at various flow rates ("capacities") and specific speeds. To obtain Ω_s, divide by 2733. (Reference 55)

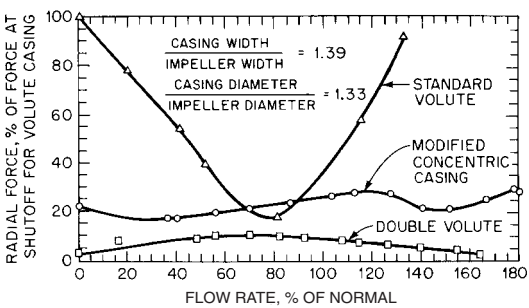

FIGURE 48 Comparison of the effect of three casing designs on radial forces for n_s = 1165 (0.426) (Reference 55)

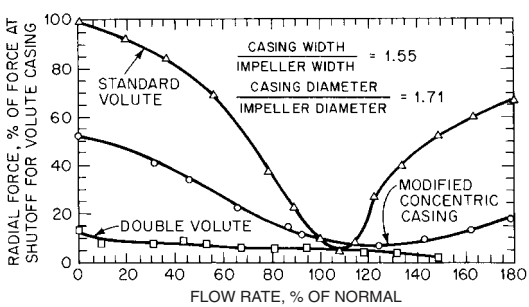

FIGURE 49 Comparison of the effect of three casing designs on radial forces for n_s = 2120 (0.776) (Reference 55)

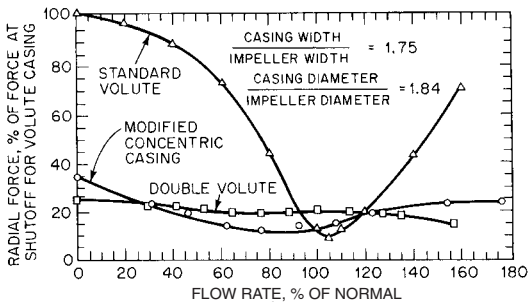

FIGURE 50 Comparison of effect of three casing designs on radial forces for n_s = 3500 (1.281) (Reference 55)

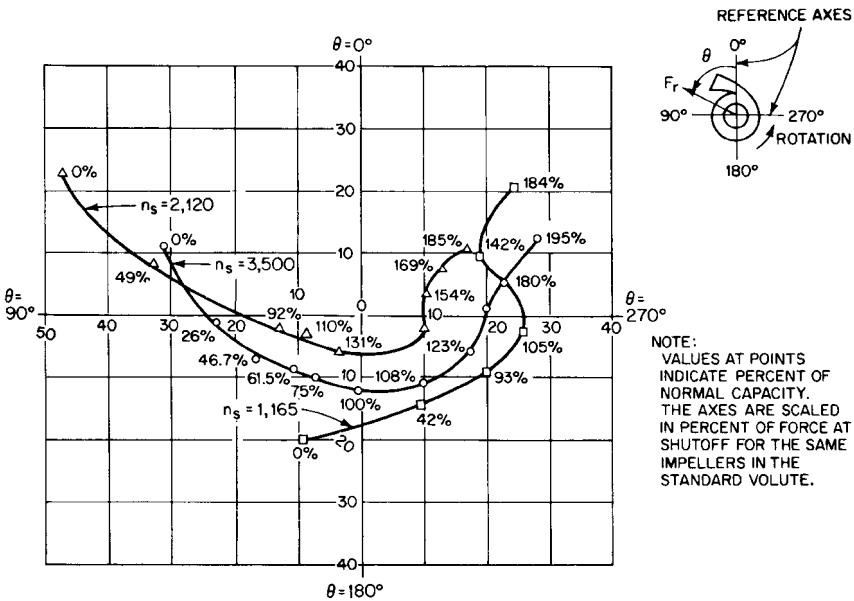

FIGURE 51 Polar plot showing direction of resultant radial forces for modified concentric casings at various flow rates and specific speeds; namely, 1,165 (0.426), 2,120 (0.776), and 3500 (1.281). The casings were concentric for 270° from the tongue. (Reference 55)

Solution

(a) K_r = 0.2 from Figure 46, by Eq. 34.

$$F_r = (0.433)(0.2)(1.0)(244)(15.125)(2.5) = 799 \text{ lb } (3554 \text{ N})$$

Estimating between the curves for n_S, = 2370 (0.867) and 1735 (0.635) in Figure 47, the direction of F_r on the shaft should be about 65° to 70° from the casing tongue in the direction of rotation.

(b) Use Figure 49, n_s = 2120 (0.776), which is nearest to n_s = 2000 (0.730), to find the radial force for a modified concentric casing at half flow, which is about 33%

of shutoff value for a single-volute casing. From Figure 46, for a single-volute casing at shutoff, $K_r = 0.34$ and

$$F_r = (0.433)(0.34)(1.0)(252)(15.125)(2.5) = 1403 \text{ lb } (6241 \text{ N})$$

Then, for a modified concentric casing at half flow,

$$F_r = (0.33)(1403) = 463 \text{ lb } (2059 \text{ N})$$

From Figure 51, the direction of F_r should be about 75° to 80° from the casing tongue in the direction of rotation.

(c) From Figure 49, the radial force for a double-volute casing is about 8% of the shutoff value for the single-volute casing, and so

$$F_r, = (0.08)(1403) = 112 \text{ lb } (499 \text{ N})$$

According to Agostinelli et al.,[55] the direction of the radial thrust in double-volute casings was found to be generally toward the casing tongue. Stepanoff[12] has found this direction to follow approximately that in single-volute casings (see also Biheller[56]).

Axial Thrust See Section 2.1 and 2.2.1.

ABNORMAL OPERATION

Complete Pump Characteristics Many types of abnormal operation involve reversed pump rotation, reversed flow direction, or both, and special tests are required to cover these modes of operation. Several methods of organizing the data have been proposed, and each has certain advantages. The Thoma diagrams shown in Figures 52 and 53[45] are easily understood and are truly *complete characteristics diagrams* because all possible modes of operation are covered (see also Reference 57).

Figure 54 shows schematic cross-sections of the two pumps tested by Swanson[58] for which characteristics are given in Figure 53.

The *Karman circle diagram* (Reference 59) attempted to show the complete characteristics as a four-quadrant contour plot of surfaces representing head and torque with speed and flow rate as base coordinates. Because the head and torque tend to infinity in two zones of operation, another diagram would be required to show the complete pump characteristics. The data presented in such a diagram are, nevertheless, adequate for almost all requirements. One example of a circle diagram is given in Figures 55 and 56. Other examples may be found in References 12, 58, and 59.

Frequently, tests with negative head and torque have been omitted so that only half of the usual circle diagram could be shown. This has been called a *three-quadrant plot,* but the information necessary to predict an event, such as possible water-column separation following a power failure, is lacking.

Power Failure Transient A sudden power failure that leaves a pump and driver running free may cause serious damage to the system. Except for rare cases where a flywheel is provided, the pump and driver usually have a rather small moment of inertia, and so the pump will slow down rapidly. Unless the pipeline is very short, the inertia of the liquid will maintain a strong forward flow while the decelerating pump acts as a throttle valve. The pressure in the discharge line falls rapidly and, under some circumstances, may go below atmospheric pressure, both at the pump discharge and at any points of high elevation along the pipeline. The minimum pressure head which occurs during this phase of the motion is called the *downsurge,* and it may be low enough to cause vaporization followed by complete separation of the liquid column. Pipelines have collapsed under the external atmospheric pressure during separation. When the liquid columns rejoin, following separation, the shock pressures may be sufficient to rupture the pipe or the pump

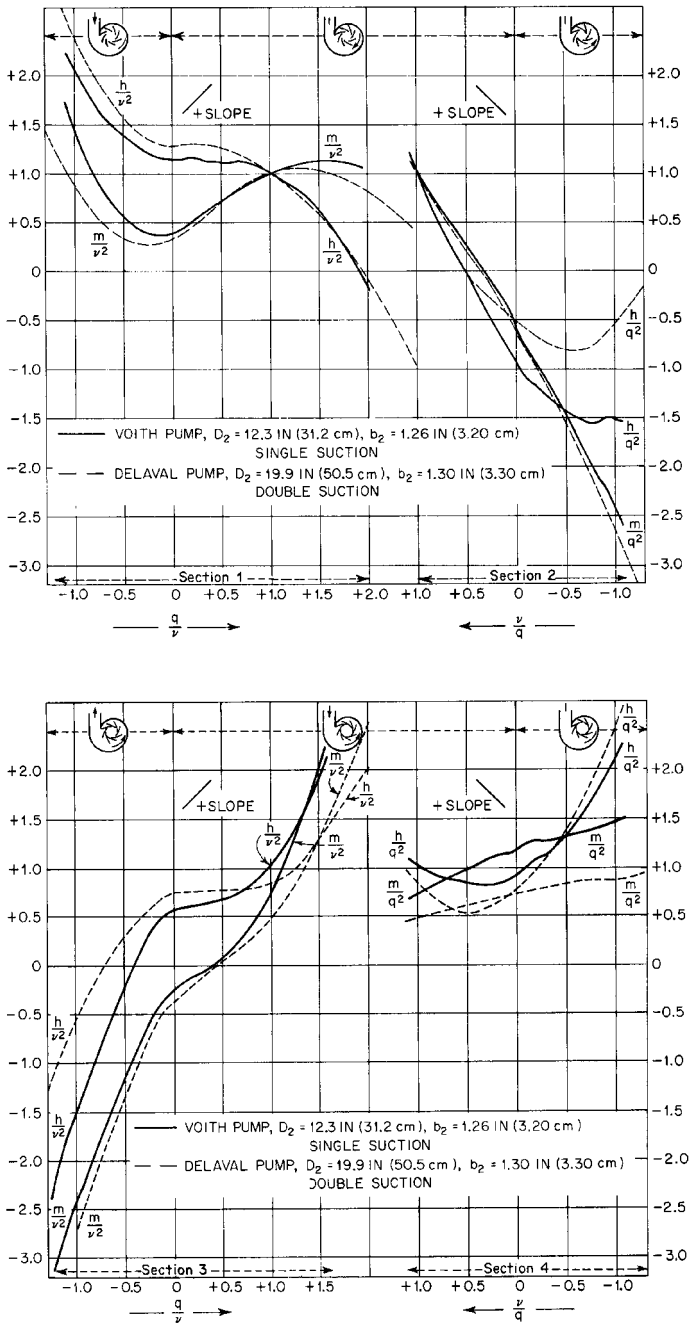

FIGURE 52 Complete pump characteristics. Specific speeds: Voith pump n_s = 1,935 (0.708); Delaval pump — n_s = 1,500 (0.549). (Reference 45)

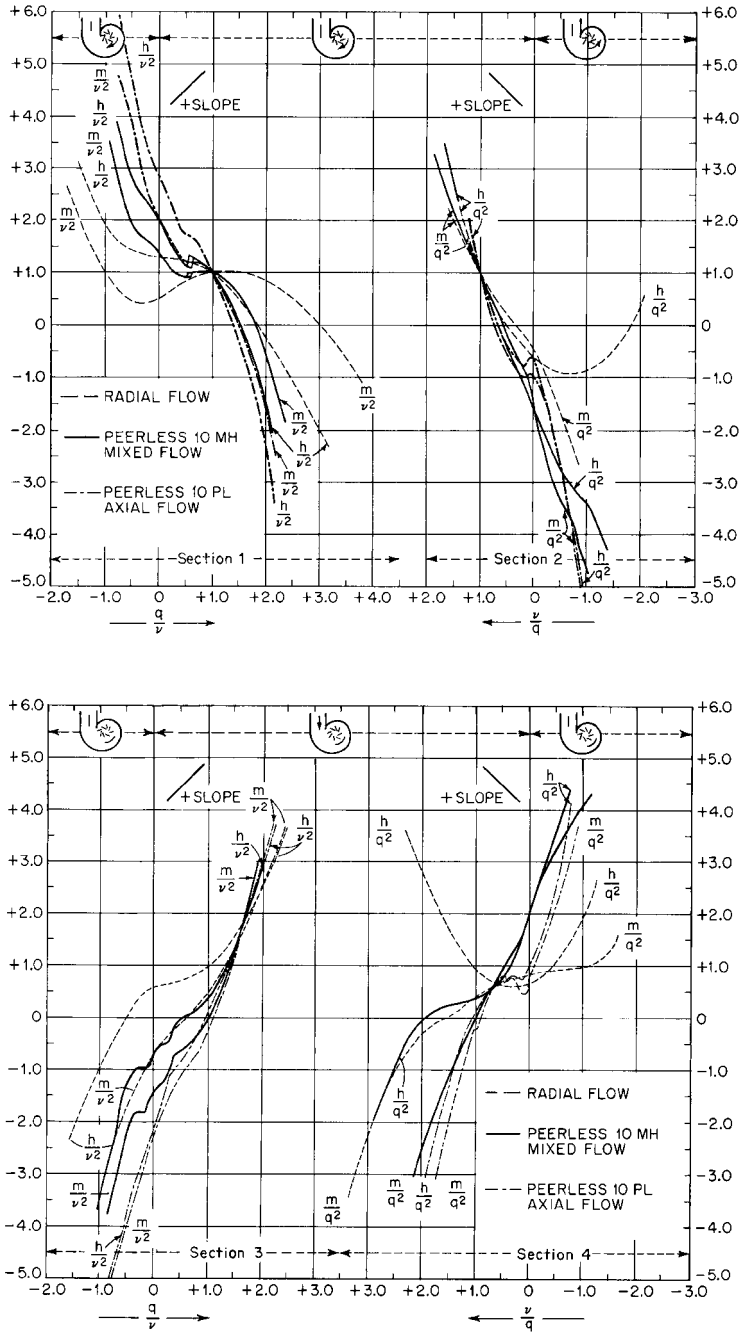

FIGURE 53 Complete pump characteristics. Specific speeds: Radial flow — n_s = 1800 (0.659); Peerless 10MH mixed flow — n_s = 7,550 (2.763); Peerless 10PL axial flow — n_s = 13,500 (4.940). (Reference 45)

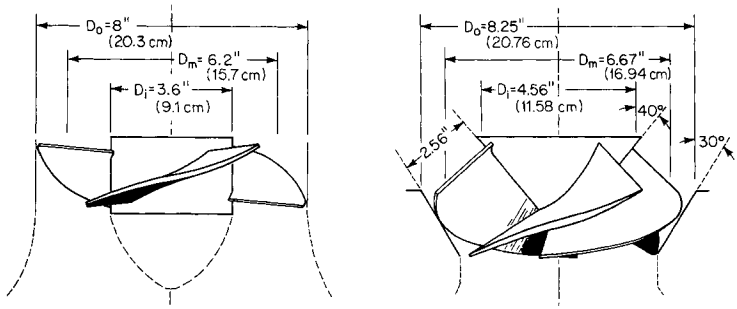

FIGURE 54 Schematic cross sections of high-specific-speed pumps. n_s = 13,500 (4.940) for axial flow pump; n_s = 7,550 (2.763) (Reference 45)

casing. Closing a valve in the discharge line will only worsen the situation, and so valves having programmed operation should be closed very little, if at all, before reverse flow begins.

Reversed flow may be controlled by valves or by arranging to have the discharge pipe empty while air is admitted at or near the outlet. If reversed flow is not checked, it will bring the pump to rest and then accelerate it with reversed rotation. Eventually the pump will run as a turbine at the runaway speed corresponding to the available static head diminished by the frictional losses in the system. However, while reversed flow is being established, the reversed speed may reach a value considerably in excess of the steady-state runaway speed. Maximum reversed speed appears to increase with increasing efficiency and increasing specific speed of the pump. Calculations indicate maximum reversed speeds more than 150% of normal speed for $n_s = 1935$ (0.708) and $\eta = 84.1\%$[45]. This should be considered in selecting a driver, particularly if it is a large electric motor.

There will be a pressure increase, called the *upsurge,* in the discharge pipe during reversed flow. The maximum upsurge usually occurs a short time before maximum reversed speed is reached and may cause a pressure as much as 60% or more above normal at the pump discharge. A further discussion of power-failure transients is given in Section 8.3.

ANALYSIS OF TRANSIENT OPERATION The data of Figures 52 and 53 have been presented in a form suitable for general application to pumps having approximately the same specific speeds as those tested. The symbols are $h = H/H_n$, $q = Q/Q_n$, $m = M/M_n$, and $\nu = n/n_n$, wherein H, Q, M, and n represent instantaneous values of head, flow rate, torque, and speed respectively and the subscript n refers to the values at best efficiency for normal constant-speed pump operation. Any consistent system of units may be used. According to the affinity laws (Eqs. 12), q is proportional to ν, and h and m are proportional to ν^2. Thus the affinity laws are incorporated in the scales of the diagrams. Figures 52 and 53 are divided into sections for convenience in reading data from the curves. The curves of sections 1 and 3 extend to infinity as q/ν increases without limit in either the positive or negative direction. This difficulty is eliminated by sections 2 and 4, where the curves are plotted against ν/q, which is zero when q/ν becomes infinite.

Usually any case of transient operation would begin at or near the point $q/\nu = \nu/q = 1$, which appears in both sections 1 and 2 of Figures 52 and 53. The detailed analysis of transient behavior is beyond the scope of this treatise. An analytical solution by the rigid column method, in which the liquid is assumed to be a rigid body, is given in Reference 45. Friction is easily included, and the results are satisfactory for many cases. The same reference includes a semigraphical solution to allow for elastic waves in the liquid, but friction must be neglected. Graphical solutions including both elastic waves and friction are discussed in References 45 to 48. Computer solutions of a variety of transient problems are discussed in Reference 47. These offer considerable flexibility in the analysis once the necessary programs have been prepared.

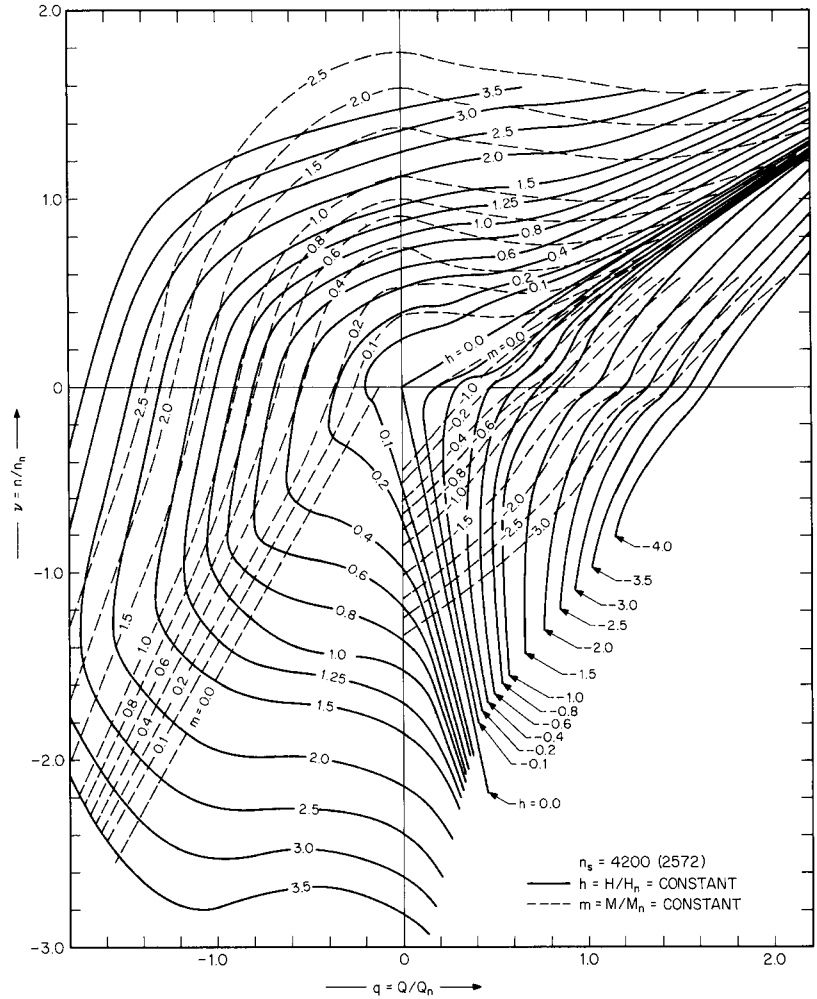

FIGURE 55 Circle diagram of pump characteristics. Specific speed n_s = 4200 (1.537). (Courtesy Combustion Engineering)

Some extreme conditions of abnormal operation can be estimated at points where the curves of Figures 52 and 53 cross the zero axes and are listed in Table 9. The data for Columns 2 to 4 of Table 9 were read from Sections 2 of Figures 52 and 53, and the data for Columns 6 and 7 were read from Sections 3. Column 8 was computed from Column 7 by assuming $h = 1$. Let the pump having $n_s = 1500$ (0.549) deliver cold water with normal head $H_n = 100$ ft (30.48 m), and let the center of the discharge flange be 4 ft (1.2 m) above the free surface in the supply sump. The discharge pressure head following power failure may be estimated by assuming the inertia of the rotating elements to be negligible relative to the inertia of the liquid in the pipeline. Then $q = 1$ and, from Column 2 of Table 9, the downsurge pressure head is (–0.22)(100) − 4 = –26 ft (–7.9 m), which is not low enough to cause separation of the water column.

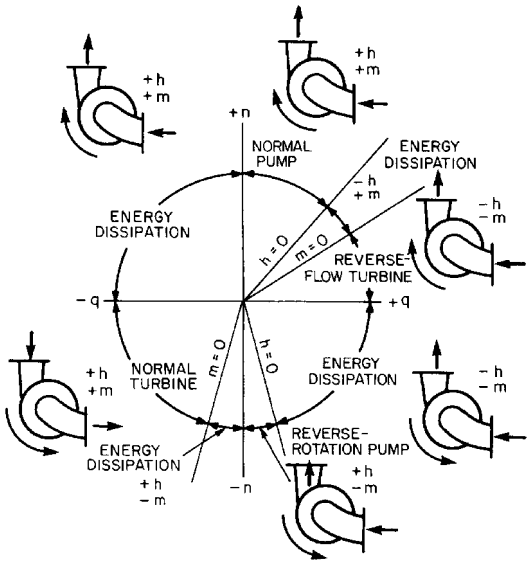

FIGURE 56 Explanatory diagram for Figure 55

TABLE 9 Abnormal operating conditions of several pumps

Specific speed n_s (Ω_s)	Downsurge				Runaway turbine		
	Free-running $m/q^2 = 0$		Locked-rotor $\nu/q = 0$		$m/\nu^2 = 0$		$h = 1$
	h/q^2	ν/q	h/q^2	m/q^2	q/ν	h/ν^2	ν
1	2	3	4	5	6	7	8
1500 (0.549)[a]	−0.22	0.36	−0.55	−0.53	0.46	0.77	1.14
1800 (0.659)	−0.24	0.31	−0.60	−0.44	0.56	0.75	1.16
1935 (0.708)	−0.36	0.32	−0.94	−0.60	0.41	0.66	1.23
7550 (2.763)	−0.23	0.56	−1.57	−1.38	0.99	0.38	1.62
13,500 (4.940)	−0.12	0.67	−0.96	−0.60	1.08	0.33	1.73

[a]Double-suction.

Actually the downsurge would be less than this because of the effects of inertia and friction, which have been neglected. If this pump were stopped suddenly by a shaft seizure or by an obstruction fouling the impeller, Column 4 of Table 9 shows the downsurge to be (–0.55)(100) − 4 = –59 feet (–18 m), which would cause water column separation and, probably, subsequent water hammer. If, following power failure, the pump were allowed to operate as a no-load turbine under the full normal pump head, Column 8 of Table 9 shows the runaway speed would be 1.14 times the normal pump speed. The steady-state runaway speed usually would be less than this because the effective head would be decreased by friction, but higher speeds would be reached during the transient preceding steady-state operation. Column 8 shows that runaway speeds increase with increasing specific speed.

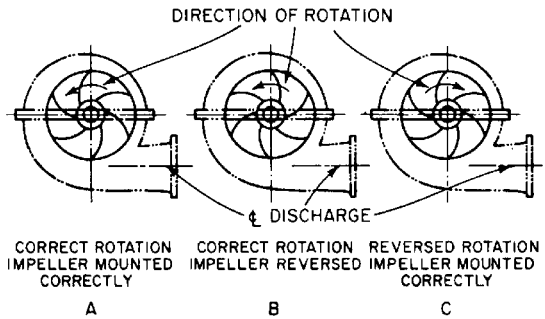

FIGURE 57A through C Pump assembly and rotation (Reference 7)

Incorrect Rotation Correct rotation of the driver should be verified before it is coupled to the pump (Figure 57). Sections 3 of Figures 52 and 53 show that reversed rotation might produce some positive head and flow rate with pumps of low specific speed, but at very low efficiency. It is unlikely that positive head would be produced by reversed rotation of a high-specific-speed pump.

Reversed Impeller Some double-suction impellers can be mounted reversed on the shaft. If the impeller is accidentally reversed, as at *B* in Figure 57, the flow rate and efficiency probably will be much reduced and the power consumption increased. Care should be taken to prevent this, as the error might go undetected in some cases until the driver was damaged by overload. Table 1 shows performance data for six pumps with reversed impellers. At least one of these would overload the driver excessively.

Further discussion of abnormal operating conditions may be found in References 7, 12, and 34.

Vibration Vibration caused by flow through wearing rings and by cavitation has been discussed in the foregoing and some remedies indicated. Vibration due to unbalance is not usually serious in horizontal units but may be of major importance in long vertical units, where the discharge column is supported at only one or two points. The structural vibrations may be quite complicated and involve both natural frequencies and higher harmonics. Vibration problems in vertical units should be anticipated during the design stage. If vibration is encountered in existing units, the following steps may help to reduce it: (1) dynamically balance all rotating elements of both pump and motor; (2) increase the rigidity of the main support and of the connection between the motor and the discharge column: (3) change the stiffness of the discharge column to raise or lower natural frequencies as required. A portable vibration analyzer may be helpful in this undertaking. Kovats[60] has discussed the analysis of this problem in some detail.

Structural vibrations can occur in most pump types. Typical sources are a) bearing housings—due to the commonly encountered cantilever construction, b) couplings, c) rotor instabilities stemming from excessive ring clearances and consequent loss of Lomakin stiffening of long-shaft multistage pumps, and d) hydraulic unbalance—due to dimensional variations in flow passages and clearances[61].

PREDICTION OF EFFICIENCY FROM MODEL TESTS

Many pumps used in pumped storage power plants and water supply projects are so large and expensive that extensive use is made of small models to determine the best design. It is often necessary to estimate the efficiency of a prototype pump, as a part of the guaran-

tee, from the performance of a geometrically similar model. A model and prototype are said to operate under dynamically similar conditions when

$$Dn/\sqrt{H} = D'n'/\sqrt{H'},$$

where D = impeller diameter
n = pump speed
H = pump head

in any consistent units of measure. Primed quantities refer to the model and unprimed quantities to the prototype. Dynamic similarity is a prerequisite to model-prototype testing so that losses that are proportional to the squares of fluid velocities, called *kinetic losses*, will scale directly with size and not change the efficiency. Surface frictional losses are boundary-layer phenomena which depend on Reynolds number

$$Re = D\sqrt{H}/\nu,$$

where ν = kinematic viscosity of the liquid pumped.

(See also Section 2.1, Eqs. 36–40.) Reynolds numbers increase with increasing size, and, within limits, surface frictional-loss coefficients decrease with increasing Reynolds number. This leads to a gain in efficiency with increasing size. Computational difficulties have forced an empirical approach to the problem. Details of the development of a number of formulas are given in Reference 62.

Moody-Staufer Formula In 1925, L. F. Moody and F. Staufer independently developed a formula that was later modified by Pantell to the form

$$\left(\frac{1 - \eta_h}{1 - \eta'_h}\right)\left(\frac{\eta'_h}{\eta_h}\right) = \left(\frac{D'}{D}\right)^n \tag{35}$$

where η_h = hydraulic efficiency, discussed previously, and D = impeller diameter. Primed quantities refer to the model, and n is a constant to be determined by tests. The model must be tested with the same liquid that will be used in the prototype; that is, cold water in most practical cases. The original formula contained a correction for head, which is negligible if $H' \geq 0.8H$, and this requirement is now virtually mandatory in commercial practice. The meager information available indicates $0.2 \geq n \geq 0.1$ approximately, with the higher value currently favored. Improvements in construction and testing techniques very likely will move n toward lower value in the future. The Moody-Staufer formula has been widely used since first publication. In practice, both η'_h and η_h are usually replaced by the overall efficiencies η' and η, respectively, because of the difficulty in determining proper values for the mechanical and volumetric efficiencies (see Eq. 11).

Rütschi Formulas The general form of several empirical formulas due to K. Rütschi[62] and others was originally given as

$$\eta_h = \frac{f}{f'}\,\eta'_h \tag{36}$$

where η_h and η'_h are the hydraulic efficiencies of the prototype and model, respectively, and f and f' are values of an empirical f function for both the prototype and the model. The f function was obtained from tests of six single-stage pumps. $n_S < 2000$ (0.732) and is shown in Figure 58 based on the *eye diameters* D_o of the pumps in *millimeters*. Thus the f function depends on actual size in addition to scale ratio. The extrapolated portion of the curve, shown dashed in Figure 58, checked well with values for a model and large prototype, shown by E' and E, respectively. One of several formulas that have been proposed to fit the curve in Figure 58 is, in SI units,

$$f = 1 - \frac{3.15}{D_o^{1.6}} \tag{37}$$

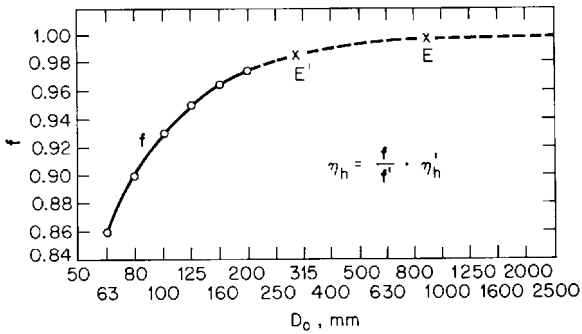

FIGURE 58 The *f* function for the Rütschi formula (to obtain D_o in inches, multiply by 0.03937) (References 13 and 62)

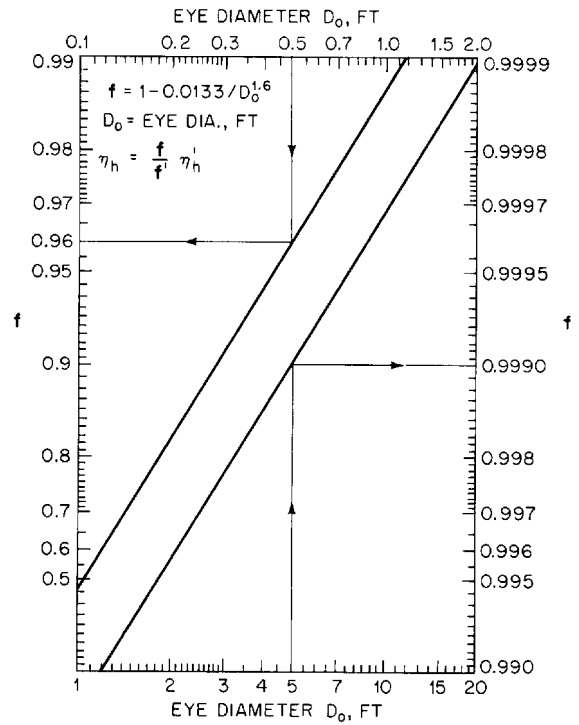

FIGURE 59 Chart for the solution of the Rütschi formula (to obtain D_o in meters, multiply by 0.3048) (Reference 62)

where the eye diameter D_o is in centimeters or, in USCS units,

$$f = 1 - \frac{0.0133}{D_o^{1.6}} \tag{38}$$

where D_o is in feet. Figure 59 gives a graphical solution of Eq. 38. The Society of German Engineers (VDI) has adopted a slightly modified version of the Rütschi formula as standard. Rütschi later recommended, in discussion of Reference 62, that the internal effi-

ciency $\eta_i = \eta/\eta_m$ be used instead of the hydraulic efficiency η_h in Eq. 45. The mechanical efficiency η_m will probably be very high for both model and prototype for most cases of interest, so good results should be obtained if the overall efficiency is used in Eq. 36.

Model-prototype geometric similarity should include surface finish and wearing ring or tip clearances, but this may be difficult or impossible to achieve. Anderson (see Section 2.1: Figure 10 and Reference 6) proposed a method that includes a correction for dissimilarity in surface finish.

OPERATION OF PUMPS AS TURBINES

Centrifugal pumps may be used as hydraulic turbines in some cases where low first cost is paramount. Because the pump has no speed-regulating mechanism, considerable speed variation must be expected unless the head and load remain very nearly constant. Some speed control could be obtained by throttling the discharge automatically, but this would increase the cost, and the power lost in the throttle valve would lower the overall efficiency.

Pump Selection After the head, speed, and power output of the turbine have been specified, it is necessary to select a pump that, when used as a turbine, will satisfy the requirements. Assuming that performance curves for a series of pumps are available*, a typical set of such curves should be normalized using the head, power, and flow rate of the best efficiency point as normal values. These curves will correspond to the right part of Section 1 of either Figure 52 or 53. In normalizing the power P, let $p = P/P_n$ and the curve of p/ν^3 will be identical with the curve of m/ν^2 in Figure 52 or 53. The normalized curves may be compared with the curves in Sections 1 of Figures 52 and 53 to determine which curves best represent the characteristics of the proposed pump. When a choice has been made, the approximate turbine performance can be obtained from the corresponding figure of Figures 60 to 63.

EXAMPLE Assume that the turbine specifications are $H_T = 20$ ft, $P_T = 12.75$ hp and $n = 580$ rpm, and that the characteristics of the DeLaval L1O/8 pump are representative of a series of pumps from which a selection can be made. The turbine discharge Q_T in gallons per minute after substituting the above values is

$$Q_T = \frac{3960P_T}{H_T\eta_T} = \frac{2520}{\eta_T} \tag{39}$$

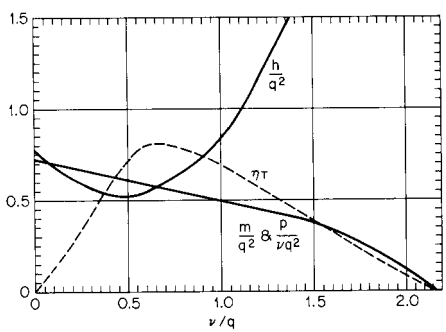

FIGURE 60 Dimensionless characteristic curves for DeLaval L 10/8 pump, constant-discharge turbine operation (Reference 63)

*It is assumed that turbine mode characteristics of the proposed pump are not available when the initial selection is made.

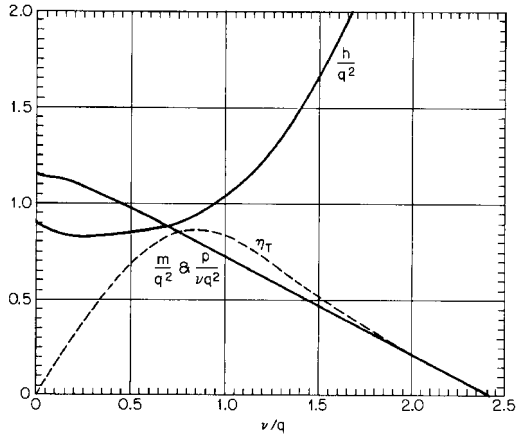

FIGURE 61 Dimensionless characteristic curves for Voith pump, constant-discharge turbine operation (Reference 63)

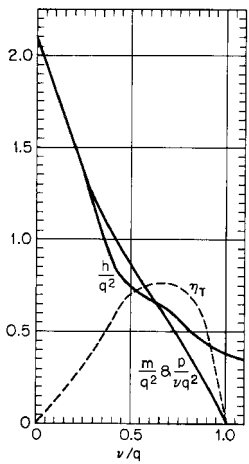

FIGURE 62 Dimensionless characteristics curves for Peerless 10MH pump, constant-discharge turbine operation (Reference 63)

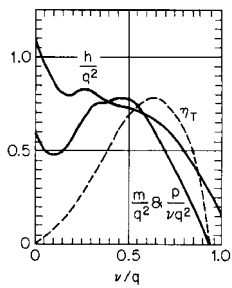

FIGURE 63 Dimensionless characteristic curves for Peerless 10PL pump, constant-discharge turbine operation (Reference 63)

where η_T is turbine efficiency, shown in Figure 60. Only the normal values Q_n, H_n P_n, and so on, are common to the curves of both Figures 52 and 60, so these alone can be used in selecting the required pump. Values of ν/q, h/q^2, and η_T are read from the curves of Figure 60 and corresponding values of Q computed by Eq. 39. Values of Q_n and H_n are then given by

$$Q_n = Q(\nu/q) \tag{40}$$

$$H_n = \frac{H(\nu/q)^2}{h/q^2} = \frac{20(\nu/q)^2}{h/q^2} \tag{41}$$

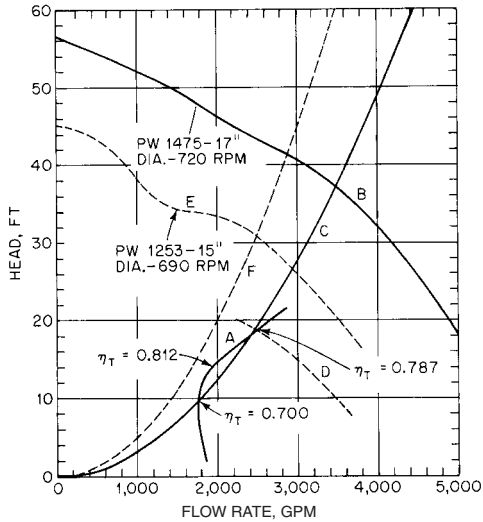

FIGURE 64 Head-flow curves of the pump selection (ft × 0.3048 = m; gpm × 0.06300 = l/s) (Reference 63)

For example, in Figure 60 at $\nu/q = 0.700$, read $h/q^2 = 0.595$ and $\eta_T = 0.805$. By Eq. 39, $Q_T = 2520/0.805 = 3130$ gpm; by Eq. 40, $Q_n = (3130)(0.700) = 2190$ gpm; and by Eq. 41, $H_n = (20)(0.700)^2/0.9595 = 16.5$ ft. In a similar manner, the locus of the best efficiency points for an infinite number of pumps, each having the same characteristics as shown in Figures 52 and 60, is obtained, and each pump would satisfy the turbine requirements. This locus of best efficiency points is plotted as curve *A* in Figure 64.

The head curve for a DeLaval L 16/14 pump having a 17-in-diameter impeller tested at 720 rpm is shown as curve *B* in Figure 64. The best efficiency point was found to be at $Q_n = 3500$ gpm and $H_n = 37.2$ ft. The locus of the best efficiency points for this pump for different speeds and impeller diameters is given by Eqs. 12 as

$$H_n = 37.2\left(\frac{Q_n}{3500}\right)^2 = \frac{3.04}{10^6}\,Q_n^2 \tag{42}$$

and is shown by curve *C* in Figure 64. Curve *C* intersects curve *A* at two points, showing that the L 16/14 pump satisfies the turbine requirements. Only the intersection at the higher turbine efficiency is of interest. At this point, $Q_n = 2490$ gpm and $H_n = 18.8$ ft. Because the turbine speed was specified to be 580 rpm, the required impeller diameter is given by Eqs. 12 as

$$D = \frac{(17)(2490/3500)}{580/720} = 15 \text{ in}$$

or by

$$D = \frac{17\sqrt{18.8/37.2}}{580/720} = 15 \text{ in}$$

The computed head curve for the 15-in-diameter impeller at 580 rpm is shown as curve *D* in Figure 64. The turbine discharge is 3200 gpm from Eq. 39 with $\eta_T = 0.787$.

The optimum solution would be to have Curve *C* tangent to Curve *A* at the point corresponding to maximum turbine efficiency, in this case $\eta_T = 0.812$. Because this

would require a smaller pump, Curve *E* in Figure 64 shows a head curve for a K 14/12 pump, which was the next smaller pump in the series. Curve *F,* the locus of the best efficiency points, does not intersect Curve *A,* showing that the smaller pump will not satisfy the turbine requirements. It is important to note that the turbine head, 20 ft, specified for this example was assumed to be the net head from the inlet to outlet flange of the pump when installed and operated as a turbine.

The procedure outlined above should lead to the selection of a pump large enough to provide the required power. However, it probably will be necessary to apply the affinity laws over such wide ranges of the variables that the usual degree of accuracy should not be expected. Considerable care should be exercised if it becomes necessary to interpolate between the curves of Figures 60 to 63. The computed performance will very likely differ from the results of subsequent tests. The curves of Figure 60 may be converted to show the constant-head characteristics of the L 16/14 pump when installed and operated as a turbine. Details of the method of computation are given in Reference 63, and the computed characteristics are shown in Figure 65.

A comprehensive study by Acres American[64,65] led to a computer program to aid in selecting a pump to meet specific requirements when operating in the turbine mode. Known pump characteristics are entered in the program according to a specified format. The computer compares them with stored characteristics of pumps for which turbine mode characteristics are known and provides estimated turbine mode characteristics for the proposed pump. Vols. I and III of Reference 64 describe the method of computation and give complete instructions for using the program.

Optimized Hydraulic Turbines A logical outgrowth of applying pumps as hydraulic turbines is the optimization of these machines as turbines. Several points of efficiency improvement have been demonstrated over that of pumps running in reverse as turbines.[66] The fluid accelerates through both the stator or nozzles and the turbine wheel or runner, whereas it decelerates through the same elements when they are acting as impeller and diffuser or volute in the pumping mode. If the fluid never has to decelerate

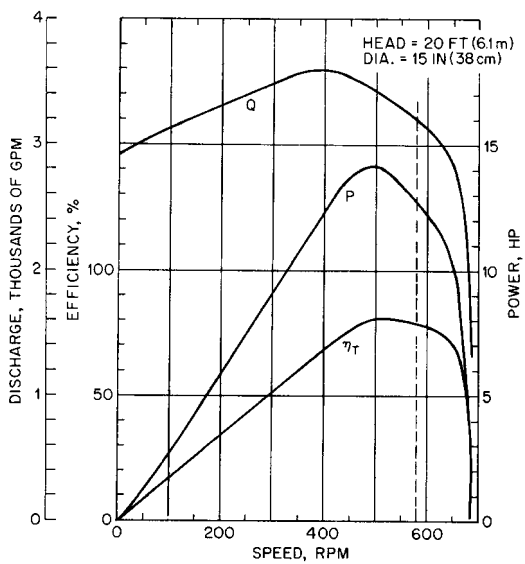

FIGURE 65 Computed constant-head turbine characteristics for DeLaval L 16/14 pump (gpm × 0.06309 = l/s; hp × 0.7457 = kW) (Reference 63)

because the turbine will never be used as a pump, the nozzles and runner can be designed to produce more aggressive and efficient acceleration in shorter distances than if the same machine is simply a pump being used as a turbine. If it is a radial-inflow runner, the resulting optimized turbine wheel employs a radial blade (with a blade angle $\beta = 90$ deg. from the tangential direction) at the outer diameter (inlet). This outer diameter is about 75% of the diameter of the impeller of the pump-as-turbine, which further improves the efficiency by reason of the reduction of the disk friction drag of the runner. Design and application of both approaches is explained and compared in Reference 67. Many of the applications of these hydraulic turbines are for power recovery in the pressure let-down processes that occur in petroleum refining. Another variable is introduced in such processes; namely, the evolution of large volumes of dissolved gas as the pressure decreases through successive stages or portions of the turbine. This phenomenon affects the performance of hydraulic turbines for such applications because somewhat more power is produced when gas evolves from the liquid than when a single-phase liquid flows through the turbine at the same pressure drop and mass flow rate.[68]

VORTEX PUMPS

A typical vortex pump is shown in Figure 66.* The ability of this type of pump to handle relatively large amounts of suspended solids as well as entrained air or gas more than offsets the relatively low efficiency. Table 10 lists performance data for four typical vortex pumps and four radial-flow centrifugal pumps of nearly the same head and flow rate. Figure 67 shows the head characteristics of a typical vortex pump with impellers of different diameters together with curves of constant efficiency and constant *NPSH*. Power curves for the same impellers are shown in Figure 68.

Curves for a conventional radial-flow pump have been added for comparison in Figures 67 and 68. Note that the head of the vortex pump does not decrease as rapidly with an increasing flow rate as does the head of the conventional pump. The power requirement of the vortex pump increases almost linearly with an increasing flow rate, whereas the power required by a conventional pump of about the same specific speed reaches a maximum and then decreases with the increasing flow rate.

Thus if the motor of the vortex pump has been selected to match the power required at the normal flow rate for best efficiency, it will be overloaded if the pump operates much beyond that point.

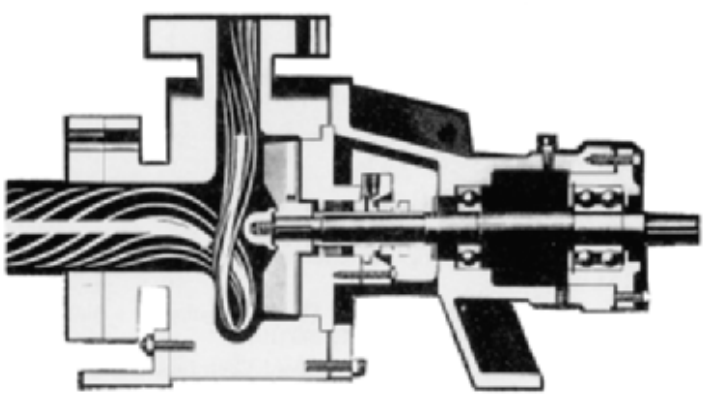

FIGURE 66 Vortex pump (courtesy Fybroc Division, METPRO)

*See also Section 9.2.

TABLE 10 Characteristics of typical vortex pumps and comparable radial-flow centrifugal pumps at 1750 rpm

Impeller	Flow rate, gpm	(l/s)	Total head, ft	(m)	Specific speed, n_s	(Ω_s)	Suction specific speed, S	(Ω_{ss})	Impeller diameter, in	(mm)	Sphere diameter,[a] in	(mm)	Efficiency[b] at $Q = Q_n$, %	Shutoff power,[b] $\%P_n$	Power[b] at $1.5Q_n$, $\%P_n$	Shutoff head,[b] $\%H_n$	Head[b] at $1.5Q_n$, $\%H_n$	NPSHR[b] at Q_n, ft	(m)	NPSHR[b] at $1.5Q_n$, ft	(m)
Vortex	100	(6.3)	24	(7.3)	1614	(0.591)	7700	(2.82)	$5\frac{7}{8}$	(149)	2	(51)	39.5	37.5	131	120	71	3	(0.9)	8	(2.4)
Radial	108	(6.8)	26	(7.9)	1580	(0.578)	6430	(2.35)	$5\frac{7}{8}$	(149)	$\frac{5}{8}$	(16)	59	50	108	144	50	4	(1.2)	7.5	(2.3)
Vortex	200	(12.6)	61	(18.6)	1134	(0.415)	7400	(2.71)	$8\frac{3}{8}$	(213)	2	(51)	45	45	129	123	82	5	(1.5)	8	(2.4)
Radial	225	(14.2)	60	(18.3)	1218	(0.446)	6450	(2.36)	$8\frac{3}{8}$	(213)	$\frac{3}{4}$	(19)	61	50	130	125	65	6.5	(2.0)	14	(3.4)
Vortex	850	(53.6)	108	(32.9)	1523	(0.557)	9820	(3.59)	$11\frac{1}{2}$	(292)	4	(102)	59	49	134	120	83	9	(2.7)	15	(4.6)
Radial	900	(56.8)	102	(31.1)	1636	(0.599)	8690	(3.18)	$11\frac{1}{2}$	(292)	$\frac{7}{8}$	(22)	76	47	113	135	44	11	(3.4)	21	(6.1)
Vortex	1050	(66.2)	150	(45.7)	1323	(0.484)	7088	(2.59)	13	(330)	$3\frac{3}{4}$	(95)	56	48	137	115	87	16	(4.9)	20	(6.1)
Radial	1250	(78.9)	154	(46.9)	1415	(0.518)			13	(330)	$1\frac{1}{32}$	(26)	83	52	123	116	45	11	(3.4)	-	(-)
Vortex average					1399	(0.512)							50	45	133	120	81				
Radial average					1462	(0.535)							70	50	119	130	51				

[a]Diameter of the largest sphere that will pass through the pump

[b]Subscript n designates values at the best efficiency point

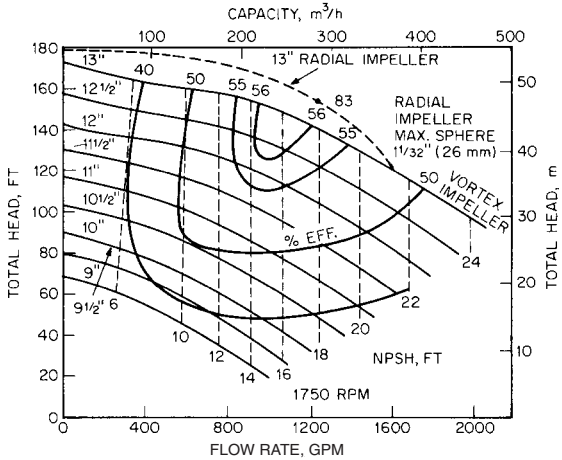

FIGURE 67 Head characteristics of a typical vortex pump. Curves show approximate characteristics when pumping clear water (in × 2.54 = cm) (Flowserve Corporation).

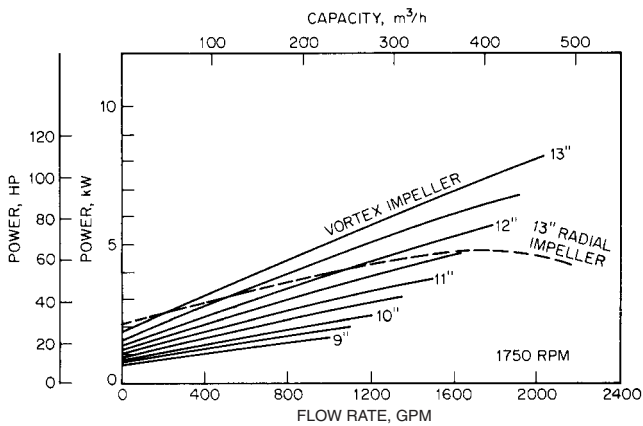

FIGURE 68 Power characteristics of a typical vortex pump. Curves show approximate characteristics when pumping clear water (in × 2.54 = cm) (Flowserve Corporation).

REFERENCES

1. Pfleiderer, C. *Die Kreiselpumpen für Flüssigkeiten und Gase.* 5te Auflage, Springer-Verlag, 1961.
2. Gülich, J., Favre, J. N., and Denus, K. "An Assessment of Pump Impeller Performance Predictions by 3D-Navier Stokes Calculations." Third International Symposium on Pumping Machinery (S239), ASME Fluids Engineering Division Summer Meeting, Paper No. FEDSM97-3341, June 1997.

3. Rupp, W. E. *High Efficiency Low Specific Speed Centrifugal Pump*. U.S. Patent No. 3,205,828, September 14, 1965.
4. Barske, U. M. "Development of Some Unconventional Centrifugal Pumps." *Proc. Inst. Mech. Eng.,* London, **174**(11):437, 1960.
5. Manson, W. W. "Experience with Inlet Throttled Centrifugal Pumps, Gas Turbine Pumps." *Cavitation in Fluid Machinery,* Symposium Publication, ASME, 1972, pp. 21–27.
6. Wislicenus, C. F. "Critical Considerations on Cavitation Limits of Centrifugal and Axial-Flow Pumps." *Trans ASME,* **78:**1707, 1956.
7. Karassik, I. J., and Carter, R. *Centrifugal Pumps: Selection, Operation and Maintenance.* McGraw-Hill, New York, 1960.
8. Holland, F. A., and Chapman, F. S. *Pumping of Liquids.* Reinhold, New York, 1966.
9. Ippen, A. T. "The Influence of Viscosity on Centrifugal Pump Performance." *Trans. ASME,* **68**(8):823, 1946.
10. Black, H. F., and Jensen, D. N. "Effects of High-Pressure Ring Seals on Pump Rotor Vibrations." ASME Paper No. 71-WA/FF-38, 1971.
11. Wood, C. M., Welna, H., and Lamers, R. P. "Tip-Clearance Effects in Centrifugal Pumps." *Trans. ASME, J. Basic Eng.,* Series D, **89:**932, 1965.
12. Stepanoff, A. J. *Centrifugal and Axial Flow Pumps*, 2nd ed., Krieger Publishing, Malabar, FL, 1957.
13. Rütschi, K. "Untersuchungen an Spiralgehäusepumpen veraschiedener Schnelläufigkeit," *Schweiz. Arch Angew, Wiss. Tech.* **17**(2):33, 1951.
14. Stepanoff, A. J. *Pumps and Blowers: Two Phase Flow.* Krieger Publishing, Malabar, FL, 1965.
15. Knapp, R. T. "Recent Investigations of the Mechanics of Cavitation and Cavitation Damage." *Trans. ASME* **77:**1045, 1955.
16. Knapp, R. T. "Cavitation Mechanics and Its Relation to the Design of Hydraulic Equipment." James Clayton, Lecture, *Proc. Inst. Mech. Eng.,* London, Sec. A, **166:**150, 1952.
17. Shutler, N. D., and Mesler, R. B. "A Photographic Study of the Dynamics and Damage Capabilities of Bubbles Collapsing Near Solid Boundaries." *Trans. ASME, J. Basic Eng.,* Series D, **87:**511, 1965.
18. Hickling, R., and Plesset, M. S. "The Collapse of a Spherical Cavity in a Compressible Liquid." Division of Engineering and Applied Sciences, Report No. 85-24, California Institute of Technology, March 1963.
19. Pilarczyk, K., and Rusak, V. "Application of Air Model Testing in the Study of Inlet Flow in Pumps." *Cavitation in Fluid Machinery,* ASME, 1965, p. 91.
20. Plesset, M. S. "Temperature Effects in Cavitation Damage." *Trans. ASME, J. Basic Eng.,* Series D, **94:**559, 1972.
21. Hammitt, F. C. "Observations on Cavitation Damage in a Flowing System." *Trans. ASME, J. Basic Eng.,* Series D, **85:**347 (1963).
22. Preece, C. M., ed. *Treatise on Materials Science and Technology.* Vol. 16, *Erosion,* Academic Press, New York, 1979.
23. Kovats, A. *Design and Performance of Centrifugal and Axial Flow Pumps and Compressors.* Macmillan, New York, 1964.
24. Palgrave, R., and Cooper, P. "Visual Studies of Cavitation in Pumping Machinery." *Proceedings of the Third International Pump Symposium,* Texas A&M University, 1986, pp. 61–68.
25. Cooper, P., Sloteman, D. P., Graf, E., and Vlaming, D. J. "Elimination of Cavitation-Related Instabilities and Damage in High-Energy Pump Impellers." *Proceedings of the Eighth International Pump Users Symposium,* Texas A&M University, 1991, pp. 3–19.

26. Vlaming, D. J. "Optimum Impeller Inlet Geometry for Minimum NPSH Requirements for Centrifugal Pumps." *Pumping Machinery—1989*, ASME, July 1989, pp. 25–29.
27. Hydraulic Institute ANSI/HI 2000 Edition Pump Standards, Hydraulic Institute, Parsippany, NJ www.pumps.org.
28. "Centrifugal Pumps." PTC 8.2-1965, American Society of Mechanical Engineers, New York, 1965.
29. Wislicenus, C. F., Watson, R. M., and Karassik, I. J. "Cavitation Characteristics of Centrifugal Pumps Described by Similarity Considerations." *Trans. ASME* **61:**17, 1939; **62:**155, 1940.
30. Stahl, H. A., and Stepanoff, A. J. "Thermodynamic Aspects of Cavitation in Centrifugal Pumps." *Trans. ASME* **78:**1691, 1956.
31. Salemann, V. "Cavitation and NPSH Requirements of Various Liquids." *Trans. ASME, J. Basic Eng.,* Series D, **81:**167, 1959.
32. Stepanoff, A. J. "Cavitation Properties of Liquids." *Trans. ASME, J. Eng. Power,* Series A, **86:**195, 1964.
33. Cooper, P. "Analysis of Single- and Two-Phase Flows in Turbopump Inducers." *Transactions of the ASME*, Series A, Vol. 89, 1967, pp. 577–588.
34. Lazarkiewicz, S., and Troskolański, A. T. *Impeller Pumps,* Pergamon Press, New York, 1965.
35. Gongwer, C. A. "A Theory of Cavitation Flow in Centrifugal-Pump Impellers." *Trans. ASME,* **63:**29, 1941.
36. Guelich, J. F. *Guidelines for Prevention of Cavitation in Centrifugal Feedpumps.* EPRI CS-6398, 1989.
37. ASTM Standard G-32. *Cavitation Erosion Using Vibratory Apparatus,* American Society for Testing Materials, 1992.
38. Cooper, P., and Antunes, F. F. "Cavitation Damage in Boiler Feed Pumps." *Symposium Proceedings: Power Plant Feed Pumps—The State of the Art*, EPRI CS-3158, July 1983, pp. 2–24 to 2–49.
39. Cooper, P., Sloteman, D. P., and Dussourd, J. L. "Stabilization of the Off-Design Behavior of Centrifugal Pumps and Inducers." *Proceedings of the Second European Congress on Fluid Machinery for the Oil, Petrochemical and Related Industries*, I Mech E Conference Publications, 1984-2, Paper No. C41/84, 1984, pp. 13–20.
40. Stripling, L. B., and Acosta, A. J. "Cavitation in Turbopumps—Part 1." *Transactions of the ASME*, Series D, Vol. 84, 1962, pp. 326–338.
41. Stripling, L. B. "Cavitation in Turbopumps—Part 2." *Transactions of the ASME*, Series D, Vol. 84, 1962, pp. 339–350.
42. Grohmann, M. "Extend Pump Application with Inducers." *Hydrocarbon Processing,* Dec. 1979, p. 121.
43. Doolin, J. H. "Centrifugal Pumps and Entrained Air Problems." *Pump World,* **4**(3), 1978.
44. *Mechanical Engineering.* **93**(6):89, 1971.
45. Kittredge, C. P. "Hydraulic Transients in Centrifugal Pump Systems." *Trans. ASME,* **78**(6):1807, 1956.
46. Parmakian, J. *Waterhammer Analysis.* Prentice-Hall, Englewood Cliffs, NJ, 1955.
47. Streeter, V. L., and Wylie, E. B. *Hydraulic Transients.* McGraw-Hill, New York, 1967.
48. Bergeron, L. *Waterhammer in Hydraulics and Wave Surges in Electricity.* Wiley, New York, 1961.
49. Addison, H. *Centrifugal and Other Rotodynamic Pumps.* 3rd ed. Chapman & Hall, London, 1966.

50. Richardson, C. A. "Economics of Electric Power Pumping." *Allis-Chalmers Elec. Rev.* **9:**20, 1944.

51. Fraser, W. H. "Flow Recirculation in Centrifugal Pumps." *Tenth Turbomachinery Symposium*. Texas A&M University, College Station, TX, 1981, p. 95.

52. Fraser, W. H. "Recirculation in Centrifugal Pumps." *Materials of Construction of Fluid Machinery and Their Relationship to Design and Performance.* ASME, November 1981, pp. 65–86.

53. Gopalakrishnan, S. "A New Method for Computing Minimum Flow." *Proceedings of the Fifth International Pump Users Symposium.* Texas A&M University, 1988, pp. 41–47.

54. "Code of Practice for Pump Efficiency Testing by the Direct Thermodynamic Method." Report 695/27, The Pump Centre, AEA Technology plc, Birchwood Science Park, Warrington WA3 6AT, UK, June 1995.

55. Agostinelli, A., Nobles, D., and Mockridge, C. R. "An Experimental Investigation of Radial Thrust in Centrifugal Pumps." *Trans. ASME, J. Eng. Power,* Series A, **82:**120, 1960.

56. Biheller, H. J. "Radial Force on the Impeller of Centrifugal Pumps with Volute, Semivolute, and Fully Concentric Casings." *Trans. ASME, J. Eng. Power,* Series A, **87:**319, 1965.

57. Donsky, B. "Complete Pump Characteristics and the Effects of Specific Speeds on Hydraulic Transients." *Trans. ASME, J. Basic Eng.,* Series D, **83:**685, 1961.

58. Swanson, W. M. "Complete Characteristic Circle Diagrams for Turbomachinery." *Trans. ASME* **75:**819, 1953.

59. Knapp, R. T. "Complete Characteristics of Centrifugal Pumps and Their Use in the Prediction of Transient Behavior." *Trans. ASME* **59:**683, 1937; **60:**676, 1938.

60. Kovats, A. "Vibration of Vertical Pumps." *Trans. ASME, J. Eng. Power,* Series A, **84:**195, 1962.

61. Bolleter, U., Leibundgut, E., Sturchler, R., and McCloskey, T. "Hydraulic Interaction and Excitation Forces of High Head Pump Impellers." *Pumping Machinery—1989*, FED-Vol. 81, ASME, 1989, pp. 187–193.

62. Kittredge, C. P. "Estimating the Efficiency of Prototype Pumps from Model Tests." *Trans. ASME, J. Eng. Power,* Series A, **90:**129, 301, 1968.

63. Kittredge, C. P. "Centrifugal Pumps Used as Hydraulic Turbines." *Trans. ASME, J. Eng. Power,* Series A, **83:**74, 1961.

64. Acres American Inc. for U.S. Department of Energy, Idaho National Engineering Laboratory, *Small Hydro Plant Development Program.* Vols. I, II, and III, subcontract No. K-1574, Oct. 1980. Available from National Technical Information Service, U.S. Department of Commerce, Springfield, VA 22161.

65. Lawrence, J. D., and Pereira, L. "Innovative Equipment for Small-Scale Hydro Developments: Waterpower '81." *An International Conference on Hydropower, Proceedings.* Vol. II, Washington, DC, June 22-24, 1981, pp. 1622–1639.

66. Cooper, P., and Nelik, L. "Performance of Multi-Stage Radial-Inflow Hydraulic Power Recovery Turbines." Paper presented at ASME Winter Annual Meeting, New Orleans, December 1984.

67. Gopalakrishnan, S. "Power Recovery Turbines for the Process Industry." *Proceedings of the Third International Pump Symposium*, Texas A&M University, 1986, pp. 3–11.

68. Hamkins, C. P., Jeske, H. O., Apfelbacher, R. and Schuster, O. "Pumps as Energy Recovery Turbines With Two-Phase Flow." *Pumping Machinery—1989*, FED-Vol. 81, ASME, 1989, pp. 73–81.

69. Kallas, D. H., and Lichtman, J. Z. "Cavitation Erosion." In *Environmental Effects on Polymeric Materials,* D. V. Rosato and R. T. Schwartz, eds., Wiley-Interscience, New York, 1968, pp. 223-280.

FURTHER READING

Anderson, H. H. *Centrifugal Pumps*, Trade and Technical Press, Surrey, England, 1980.

Brennen, C. E. *Hydrodynamics of Pumps*, Concepts ETI, Inc., and Oxford University Press, 1994.

Carter, R. "How Much Torque Is Needed to Start Centrifugal Pumps?" *Power* **94**(1):88, 1950.

Church, A. H. *Centrifugal Pumps and Blowers.* Krieger Publishing, Malabar, FL, 1944.

Heald, C. C. *Cameron Hydraulic Data,* 18th ed., 1998. Flowserve Corporation, Irving, TX 75039.

Japikse, D., Marscher, W. D., and Furst, R. B. *Centrifugal Pump Design and Performance*. Concepts ETI, Inc., Wilder, VT, 1997.

Moody, L. F., and Zowaki, T. "Hydraulic Machinery." 3rd ed., sec. 26 of *Handbook of Applied Hydraulics.* Davis and Sorenson, eds., McGraw-Hill, New York, 1969.

Spanohake, W. *Centrifugal Pumps, Turbines, and Propellers.* Technology Press, MIT, Cambridge, MA, 1934.

Wislicenus, C. F. *Fluid Mechanics of Turbomachinery.* Dover, New York, 1965.